Science Signaling

1 JULY 2025

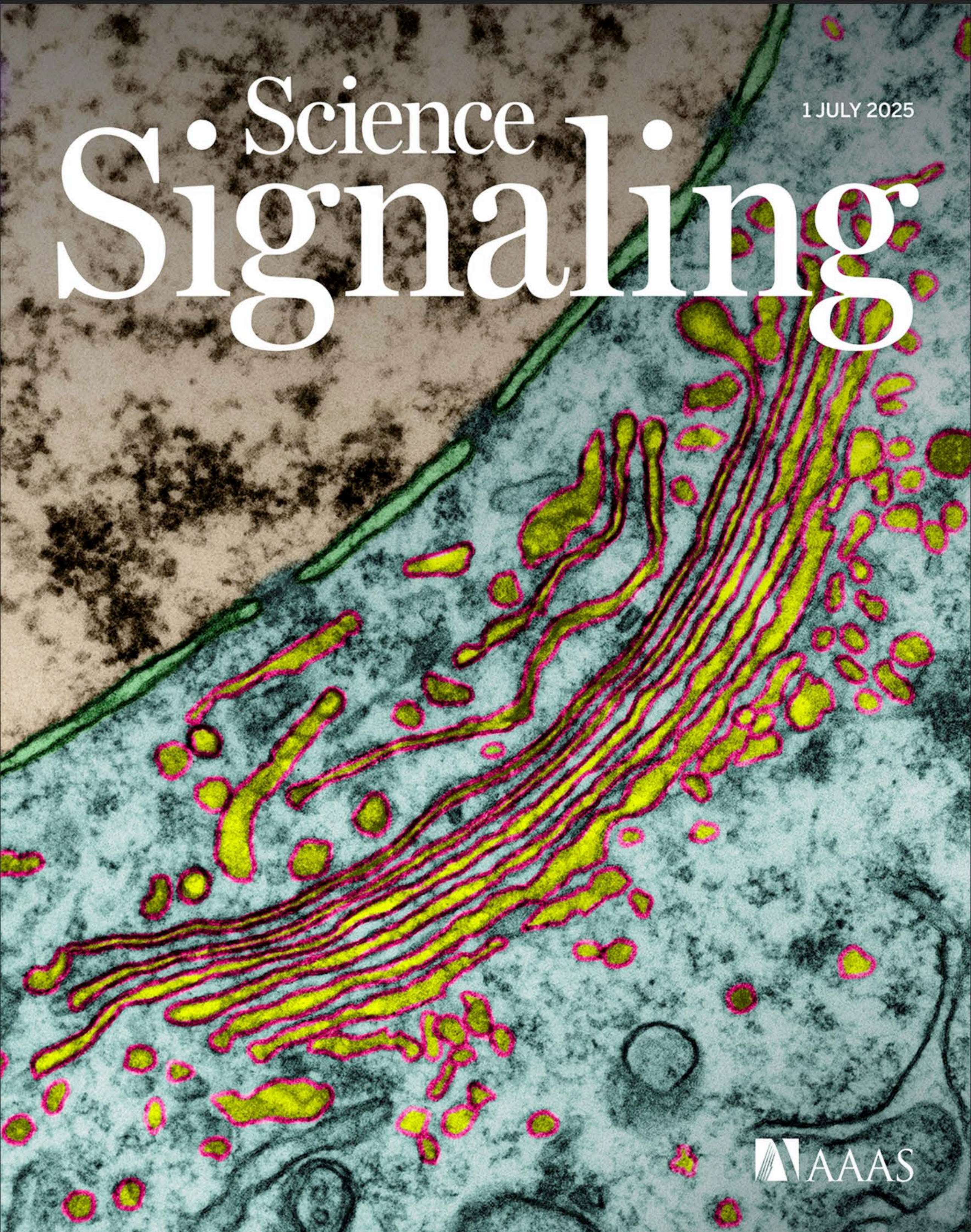

BIOCHEMISTRY

A PKCη missense mutation enhances Golgi-localized signaling and is associated with recessively inherited familial Alzheimer's disease

Maria Celeste Gauron[1]†, Dmitry Prokopenko[2,3]†, Sanghun Lee[4,5]†, Sarah A. Wolfe[1], Julian Hecker[3,6], Julian Willett[2,3], Mohammad Waqas[2], Gema Lordén[1], Yimin Yang[1], Joshua E. Mayfield[1], Isabel Castanho[3,7], Kristina Mullin[2], Sarah Morgan[7,8], Georg Hahn[5], Dawn L. Demeo[3,6], Winston Hide[3,7], Lars Bertram[9,10], Christoph Lange[3,5], Alexandra C. Newton[1]*, Rudolph E. Tanzi[2,3]*

The identification of Alzheimer's disease (AD)–associated genomic variants has provided powerful insight into disease etiology. Genome-wide association studies (GWASs) of AD have successfully identified previously unidentified targets but have almost exclusively used additive genetic models. Here, we performed a family-based GWAS of a recessive inheritance model using whole-genome sequencing from families affected by AD. We found an association between AD risk and the variant rs7161410, which is located in an intron of the *PRKCH* gene encoding protein kinase C eta (PKCη). In addition, a rare *PRKCH* missense mutation, K65R, was in linkage disequilibrium with rs7161410 and was present in homozygous carriers of the rs7161410 risk allele. In vitro analysis revealed that the catalytic rate, lipid dependence, and peptide substrate binding of the purified variant were indistinguishable from those of the wild-type kinase. However, cellular studies revealed that the K65R PKCη variant had reduced cytosolic activity and, instead, enhanced localization and signaling at the Golgi. Moreover, the K65R variant had altered interaction networks in transfected cells, particularly with proteins involved in Golgi processes such as vesicle transport. In human brain tissue, the AD-associated recessive genotype of rs7161410 was associated with increased expression of *PRKCH*, particularly in the amygdala. This association of aberrant PKCη signaling with AD and the insight into how its function is altered may lead to previously unidentified therapeutic targets for prevention and treatment.

INTRODUCTION

Alzheimer's disease (AD) is the most common form of dementia, accounting for 60 to 80% of cases in the elderly. AD is expected to increase worldwide to 66 million by 2030 and 131 million by 2050 (*1*). AD is a heterogeneous, neurodegenerative disorder broadly classified into two subtypes: early onset and late onset. Early-onset familial AD (EOAD) is generally inherited in an autosomal dominant pattern due to mutations in *APP* (*amyloid precursor protein*), *PSEN1* (*presenilin 1*), and *PSEN2* (*presenilin 2*) genes; however, there are also cases of EOAD that cannot be linked to any of these three genes. About 90% of EOAD cases from 32 US AD centers were reported to be due to autosomal recessive causes (*2*). The inheritance pattern of late-onset AD (LOAD) is polygenic, with the *APOE* (*apolipoprotein E*) ε4 allele being the strongest genetic risk factor (*3*). To date, various genes implicated in AD have been identified by genome-wide association studies (GWASs) using an additive model (AM) of inheritance, assuming a uniform and linear increase in risk (*4*, *5*). Here, to broaden our capture of AD-associated risk variants, we performed a family-based GWAS of a recessive model (RM) using whole-genome sequencing (WGS) data to trace potential recessive loci that confer susceptibility to AD. Using this model, we identified a variant in a protein kinase C (PKC) gene family member, *PRKCH*, encoding protein kinase C eta (PKCη), as a risk factor for AD. Further analysis led to the identification of rare and highly penetrant AD-associated variants resulting in missense mutations in *PRKCH* that alter function.

PKCη is a member of the novel class of PKC isozymes, Ser/Thr kinases, that are activated by the second messenger diacylglycerol (DG) (*6*–*8*). Novel PKC isozymes are closely related to the conventional PKC isozymes, which are additionally regulated by Ca^{2+}. Originally identified in the brain, conventional PKC family members are being increasingly recognized as key players in maintaining normal brain function (*9*). These isozymes regulate synapse morphology, receptor turnover, and cytoskeletal integrity. Unbiased phosphoproteomics analyses identify enhanced signaling by PKC as one of the earliest events in the pathology associated with AD (*10*). Our previous genetic analyses identified the conventional isozyme PKCα as a driver in the pathology of AD. Specifically, highly penetrant variants of the PKCα gene, *PRKCA*, which conferred increased risk for AD, were shown to be gain-of-function mutations (*11*). Introduction of one such variant (PKCα M489V) in a mouse model was sufficient to rewire the brain phosphoproteome, reduce spine

[1]Department of Pharmacology, University of California, San Diego, La Jolla, CA 92093-0721, USA. [2]Genetics and Aging Research Unit and the McCance Center for Brain Health, Department of Neurology, Massachusetts General Hospital, Charlestown, MA 02129, USA. [3]Harvard Medical School, Boston, MA 02115, USA. [4]Department of Medical Consilience, Graduate School, Dankook University, Yongin-si, 16890, South Korea. [5]Department of Biostatistics, Harvard T. H. Chan School of Public Health, Boston, MA 02115, USA. [6]Channing Division of Network Medicine, Brigham and Women's Hospital, Boston, MA 02115, USA. [7]Department of Pathology, Beth Israel Deaconess Medical Center, Boston, MA 02115, USA. [8]Blizard Institute, Department of Neuroscience, Surgery and Trauma, Queen Mary University of London, London E1 4NS, UK. [9]Lübeck Interdisciplinary Platform for Genome Analytics, Institutes of Neurogenetics and Cardiogenetics, University of Lübeck, 23562 Lübeck, Germany. [10]Center for Lifespan Changes in Brain and Cognition, Department of Psychology, University of Oslo, 0373 Oslo, Norway.
†These authors contributed equally to this work.
*Corresponding author. Email: anewton@health.ucsd.edu (A.C.N.); tanzi@helix.mgh.harvard.edu (R.E.T.)

density of neurons, enhance amyloid-β–induced synaptic depression, and cause cognitive decline (*12*). In addition, variants in another conventional PKC member, *PRKCG*, encoding Purkinje cell–localized PKCγ, are causative for spinocerebellar ataxia–type 14, likely resulting from enhanced basal signaling (*13*, *14*). However, unlike conventional isozymes, whether novel PKCs drive neurodegenerative diseases has not been previously established.

Here, using an RM of inheritance in a family-based GWAS of WGS data, we identified PKCη as a previously unreported potential target for treating AD. Specifically, we identified an intronic variant in *PRKCH*, rs7161410, to be strongly associated with AD risk. In addition, we identified five exonic variants in strong linkage disequilibrium (LD) with the risk allele rs7161410; of these, only one was present in homozygous carriers of rs7161410. This variant corresponds to a missense mutation, K65R, in a surface-exposed residue in the C2 domain of PKCη. In vitro kinase assays revealed that this mutation does not alter the intrinsic biochemical properties of PKCη. In contrast, cellular studies using fluorescence resonance energy transfer (FRET)–based reporters revealed that the mutation leads to enhanced localization and signaling of PKCη at the Golgi. In summary, performing a family-based GWAS of WGS data using an RM of inheritance, we identified a previously unknown AD-associated variant in tight LD with a missense mutation in *PRKCH* that alters PKCη function.

RESULTS

Identification of *PRKCH* as an AD marker

The AD families included in this study originated from two cohorts: the National Institute of Mental Health (NIMH) (*15*) and the family component of the National Institute of Aging AD Sequencing Project (NIA ADSP) (*16*). By design, carriers of ε4/ε4 were not included in the sequencing efforts of NIA ADSP. After the quality control filtering, two WGS familial AD cohorts with 1393 individuals (NIMH; 446 multiplex families) and 854 individuals (NIA; 159 multiplex families) were merged. In the NIMH cohort, the majority (95.33%; 1328 of 1393) were European American, and 68.05% were women: 948 patients with AD (mean age at onset or screening, 72 years; range 31 to 100) and 445 unaffected individuals. In the NIA ADSP cohort, European American, Caribbean Hispanic, and Dutch ancestry were represented and 63.11% were women: 543 patients with AD (mean age at onset or screening, 72 years; range 30 to 90), 296 unaffected individuals, and 15 patients with an unknown phenotype. Among a total of 1509 patients with AD from 605 families, the number of EOAD (onset age < 65) and LOAD (onset age ≥ 65) were 246 and 1263, respectively.

Genome-wide family-based association test (FBAT) results for RM are shown in quantile-quantile and Manhattan plots without evidence of spurious inflation of association test statistics ($\lambda = 1.00$; Fig. 1, A and B). The peak association originated on chromosome 19 and is about 500 bases downstream (3′) of *APOC1* (*apolipoprotein C1*) at 19q13.32. The top single-nucleotide polymorphisms (SNPs) rs4420638 and rs56131196, with a P_{rec} of 3.48×10^{-11}, were much more significant for AM ($P_{add} = 4.44 \times 10^{-15}$ and $P_{add} = 6.66 \times 10^{-15}$, respectively; Fig. 1C and table S1), where P_{rec} and P_{add} are the *P* value for the analysis of the recessive model and *P* value for the analysis of the additive model, respectively. We also confirmed that rs429358 (coding for the ε4 allele) in *APOE* shows a recessive signal implying a strong AD effect in carriers of the ε4/ε4 genotype (family size: 54 in RM versus 144 in AM and $P_{rec} = 4.18 \times 10^{-9}$ versus $P_{add} = 1.11 \times 10^{-15}$).

Among the loci exhibiting suggestive genome-wide significance ($P < 5 \times 10^{-7}$) for RM, only rs7161410, an intronic variant of *PRKCH* (encoding PKCη) in chromosome 14, was more significant compared with AM ($P_{rec} = 1.41 \times 10^{-7}$ versus $P_{add} = 9.20 \times 10^{-5}$, respectively; Fig. 1, B to D, and table S1), suggesting that this signal is stronger for a recessive inheritance model. Moreover, the number of informative families was much smaller for RM compared with AM (36 versus 139, respectively). Despite the considerable discrepancy in size, the *P* value was notably more significant for RM, indicating a strong recessive signal. Notably, the stratified analysis by ancestry revealed that the signal was the strongest with small informative family sizes in the Dominican families subgroup ($n = 412$, number of informative families = 10, and $P_{rec} = 7.81 \times 10^{-7}$; table S2), whereas it was significant in non-Hispanic white except Dominican families ($n = 1717$, number of informative families = 24, and $P_{rec} = 3.72 \times 10^{-3}$; table S2). However, it was not significant in African Americans ($n = 84$, number of informative families = 2, and $P_{rec} = 0.617$; table S2). The FBAT interaction test (FBAT-GE) (*17*, *18*) showed a significant interaction ($P = 0.022$) between the SNP and a binary indicator, whether or not a participant belonged to the Dominican families subgroup.

Although this allele exhibited association with AD in a family-based WGS sample in Dominican and non-Hispanic white families, we were unable to replicate this recessive association signal in an independent NIA ADSP case-control dataset, $P_{rec} = 0.89$ in African American subpopulation ($n = 4263$), $P_{rec} = 0.27$ in non-Hispanic white subpopulation ($n = 9609$), $P_{rec} = 0.65$ in Hispanic subpopulation ($n = 8466$), and $P_{rec} = 0.58$ in Asian subpopulation ($n = 2543$), and in two biobanks with an AD-by-proxy phenotype (UK Biobank, $P_{rec} = 0.57$; All of Us, $P_{rec} = 0.25$).

Next, we set out to identify exonic variants exhibiting potential functional effects, which could, in part, explain the recessive association of the intronic *PRKCH* variant with familial AD. Five SNPs were found to be in tight LD (LD, $D' > 0.9$) with the rs7161410 risk allele, all having predicted moderate or high impact on *PRKCH* (Fig. 2A). These corresponded to A19V and K65R in the C2 domain, R149Q in the C2-C1A linker, and V374I and A410S in the kinase domain (Fig. 2B). Among these variants, one missense mutation, K65R [$P_{add} = 0.074$, P_{rec} = not available (NA) because there were no homozygous carriers], which was present only in eight affected heterozygous carriers in the NIMH AD families, was of particular interest. It was the only functional mutation in *PRKCH* for which carriers were also homozygous for the minor allele of rs7161410 in both datasets—NIA ADSP unrelated patients and NIMH and NIA ADSP families—partially accounting for the observed recessive association signal with rs7131410 (table S3 and fig. S1). The removal of K65R carriers and their families from the dataset led to a slight decrease in the recessive signal of rs7161410 because of removal of one informative non-Hispanic white family, which contributed to the FBAT test statistic of rs7161410 (table S2). In addition, K65R was replicated in the latest release of NIA ADSP (v9) with unrelated cases and controls ($P_{add} = 0.030$, P_{rec} = NA because there were no homozygous carriers) in which nine carriers of K65R were homozygous for rs7161410. Among other functional mutations, V374I had 39 carriers who were homozygous for the minor allele of rs7161410 in NIA ADSP unrelated patients but not in NIMH and NIA ADSP families. The mapping of the five mutations onto the modeled structure of PKCη (*19*) revealed that these are all surface-exposed residues (Fig. 2C). Gene-based analysis including the five functional

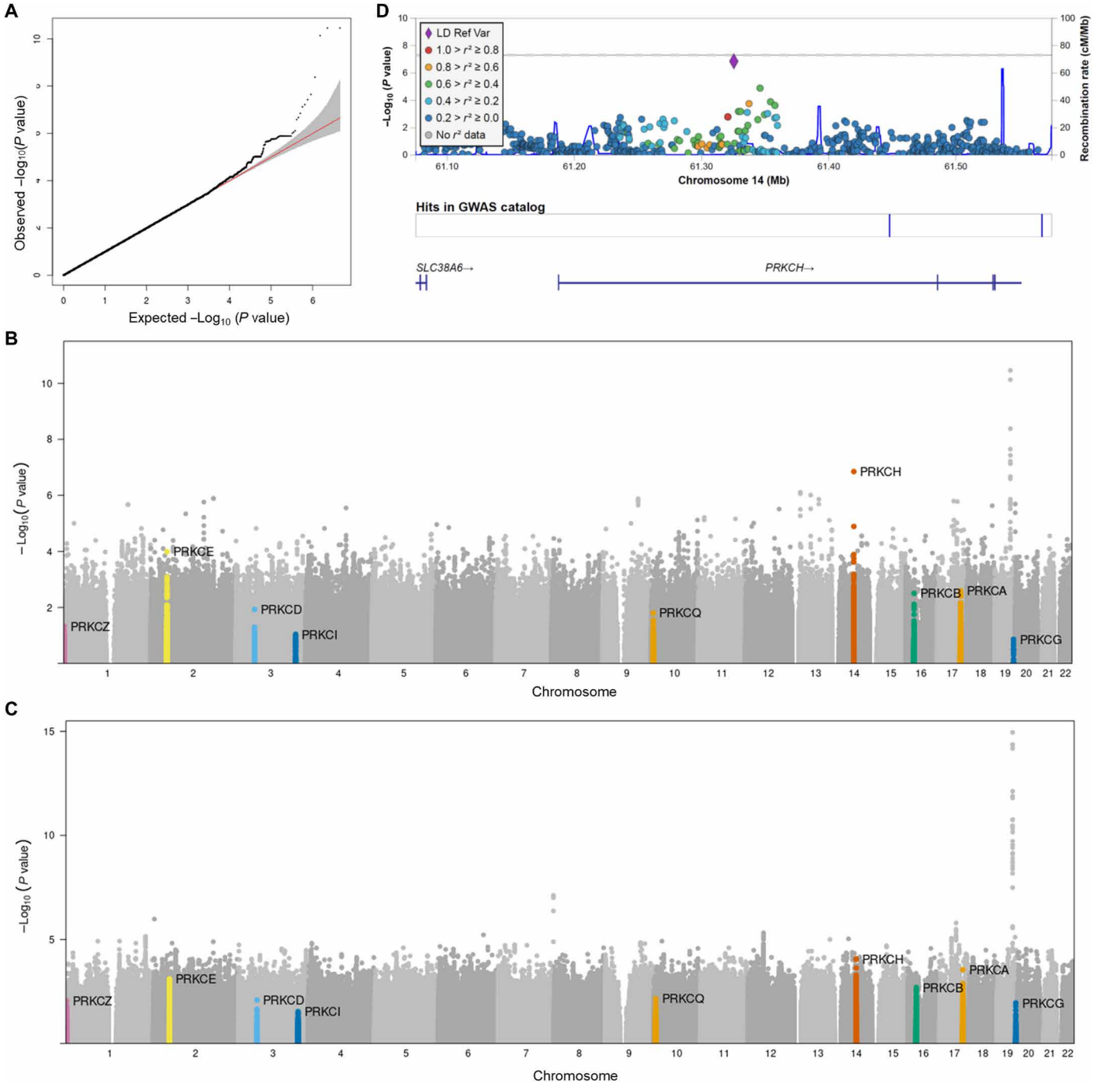

Fig. 1. Identification of *PRKCH* as an AD marker. (**A** to **D**) GWASs on 2247 patients from 558 families according to AD affection status for RM and AM. (A) Quantile-quantile plot of the recessive GWAS. (B) Manhattan plot of the recessive GWAS. (C) Manhattan plot of the additive GWAS. (D) Regional plot of the recessive significant variant rs7161410 on *PRKCH*. PKC family members are highlighted in each Manhattan plot.

mutations demonstrated significant association in the sequence kernel association test (SKAT)/variance-component–based region tests ($P_{add} = 0.0175$).

Reduced cytosolic activity of AD-associated PKCη mutations

To assess whether these AD-associated mutations affect PKCη function, we first addressed their effect on the basal and agonist-evoked activity of PKCη. We used the genetically encoded cytosolic FRET-based biosensor C kinase activity reporter 2 (CKAR2) to monitor PKC activity in the cytosol (*20*). COS7 cells coexpressing CKAR2 together with mCherry-tagged PKCη wild type (WT) or each of the five AD variants (A19V, K65R, R149Q, V374I, and A410S) were treated (i) directly with the PKC inhibitor Gö6983 to abolish PKC activity (Fig. 3, A and B) or (ii) first with uridine 5′-triphosphate

A

rsID	Chr	Position	Ref	Alt	Annotation	Impact	Gene	HGVS.p	*P* value (NIMH only)*	R^2 in NIMH	D' in NIMH
rs55645551	14	61322157	**C**	**T**	missense_variant; structural_interaction_variant	Moderate	*PRKCH*	**p.Ala19Val**	0.182	6.0E−04	1.0
rs55737090	14	61322295	**A**	**G**	missense_variant	Moderate	*PRKCH*	**p.Lys65Arg**	0.074	8.7E−03	1.0
rs55848048	14	61443129	**G**	**A**	missense_variant	Moderate	*PRKCH*	**p.Arg149Gln**	0.317	2.4E−04	1.0
rs2230500	14	61457521	**G**	**A**	missense_variant	Moderate	*PRKCH*	**p.Val374Ile**	0.033	5.1E−03	0.954
rs1884838413	14	61457629	**G**	**T**	missense_variant	Moderate	*PRKCH*	**p.Ala410Ser**	0.221	4.8E−04	1.0

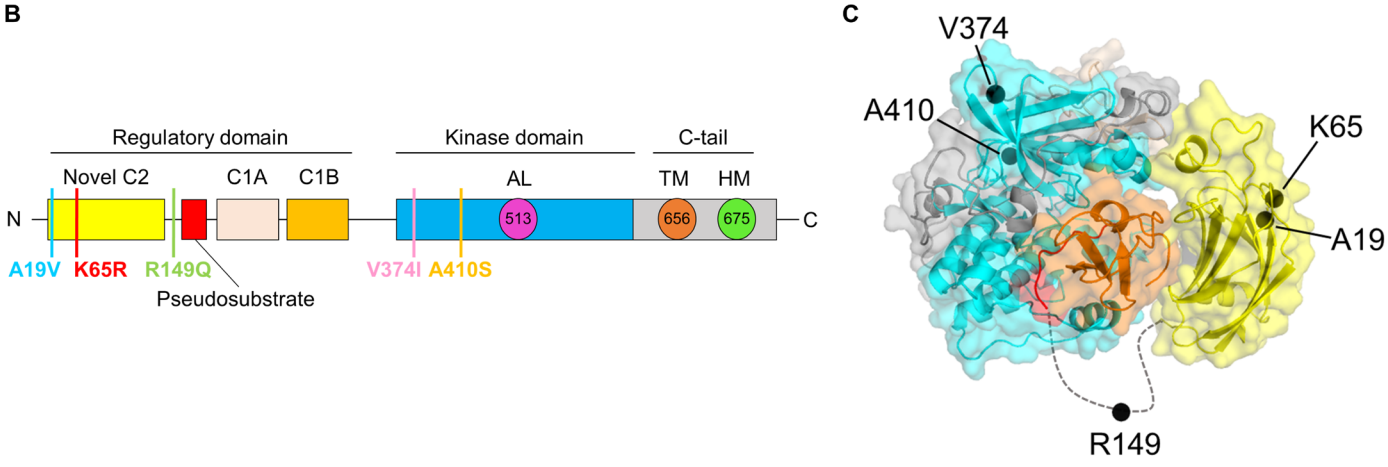

Fig. 2. PKCη AD-associated variants. (**A**) Single-nucleotide variants in linkage disequilibrium (LD, $D' > 0.9$) with rs7161410 with a moderate or high functional impact. (**B**) Primary structure of PKCη showing domain composition and position of AD-associated variants; novel C2 domain (yellow), autoinhibitory pseudosubstrate (red), C1A domain (tan), DG-sensing C1B domain (orange), kinase domain (cyan), and C-terminal tail (gray). Processing phosphorylation sites at the activation loop (Thr^{513}), turn motif (Thr^{656}), and hydrophobic motif (Ser^{675}) are indicated. (**C**) Model for autoinhibited conformation of the novel PKCη isozyme (*19*) showing the position of AD variants; residues are all surface exposed.

(UTP), which activates purinergic receptors to elevate DG (and Ca^{2+}) to transiently activate PKC, followed by treatment with Gö6983 to abolish its activity (Fig. 3, C and D). Cells expressing similar levels of mCherry PKC were selected for analysis. Unlike conventional PKC isozymes, novel PKC isozymes have high basal signaling in the absence of stimulation, which can be assessed by measuring the reduction in FRET upon PKC inhibition. The addition of Gö6983 to cells transfected with the mCherry empty vector to study the activity of endogenous PKCs caused no significant change in FRET (Fig. 3A, gray trace) because the main cytosolic activity in COS7 cells is driven by conventional PKCs, which are tightly autoinhibited in the absence of agonist stimulation. In contrast, inhibitor treatment caused a significant reduction in the FRET ratio in cells overexpressing PKCη WT (Fig. 3A, blue trace), reflecting its high basal activity in the absence of agonists. When analyzing the AD-associated mutants, it was observed that each of the five variants had significantly lower basal activity than PKCη WT (Fig. 3, A and B). These data reveal that the AD-associated mutants have lower basal signaling assessed using the cytosolic biosensor compared with PKCη WT.

We next sought to analyze the agonist-evoked activity of PKCη WT compared with the rare variants. Cells coexpressing cytosolic CKAR2 and mCherry-PKCη WT or each one of the variants were treated with UTP to stimulate DG-dependent activity and then treated with Gö6983 to abolish activity (Fig. 3C). UTP treatment caused an increase in the activity of endogenous PKC, which rapidly decayed to baseline levels, consistent with the rapid inactivation kinetics of the endogenous conventional PKC isozymes that is driven by rapid metabolism of DG (*21*). The high basal activity of PKCη WT and the AD-associated variants was further increased upon UTP treatment and was sustained, consistent with our previous report of novel PKC isozyme activity remaining sustained over time after UTP stimulus, driven by persistent DG (*21*). The agonist-evoked activity of the variants was not significantly different from that of PKCη WT (Fig. 3D). Together, our data suggest that these AD-associated mutations in PKCη exhibit activation kinetics similar to that of the WT protein but have a lower signaling output assessed with the cytosolic biosensor.

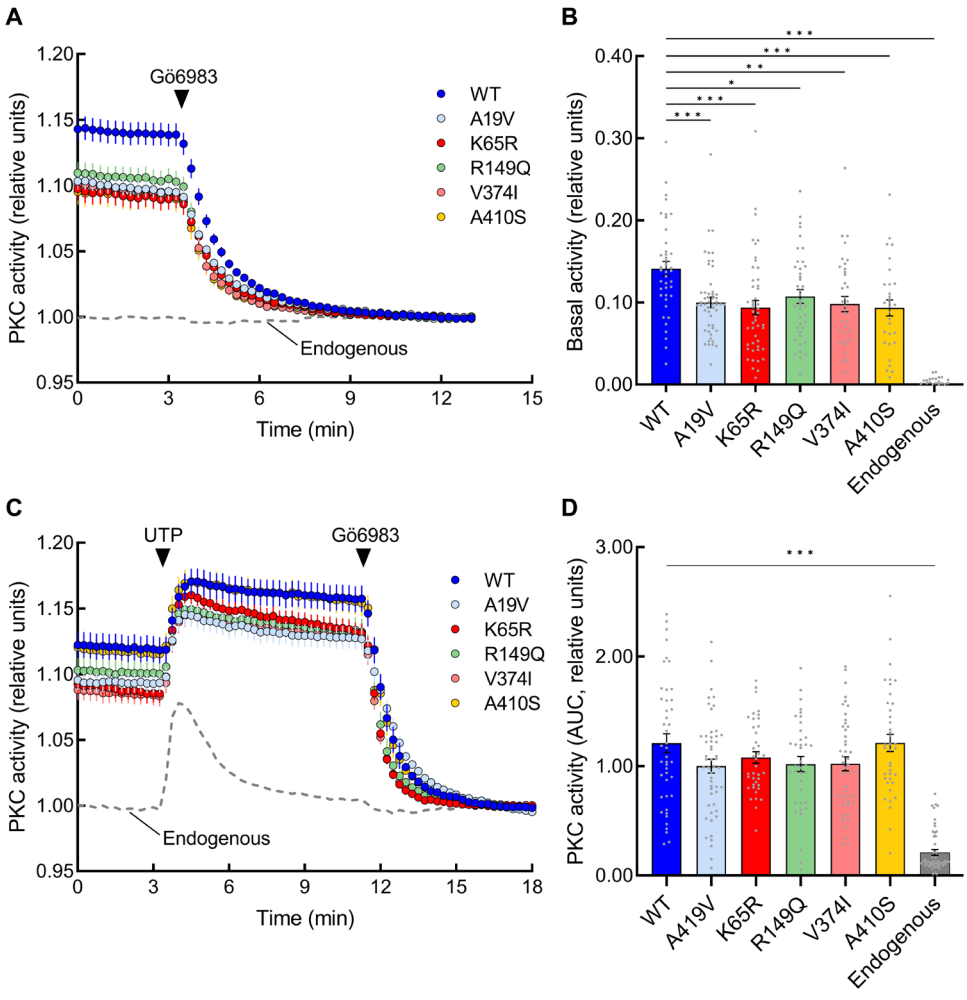

Fig. 3. AD-associated PKCη mutations have reduced activity in the cytosol. (**A**) Normalized FRET ratios representing PKC activity in COS7 cells coexpressing the indicated mCherry-tagged PKCη (WT, blue trace; A19V, cyan trace; K65R, red trace; R149Q, green trace; V374I, pink trace; A410S, yellow trace) or mCherry empty vector (endogenous PKCs, gray trace) and the PKC activity reporter cytosolic CKAR2. After establishing a baseline for 3 min, cells were treated with 1 μM of the PKC inhibitor Gö6983, indicated by the black arrow. Data are representative of 30 to 53 cells per condition, from three independent experiments. (**B**) Relative basal activity quantified using the traces in (A) by subtraction of the average of the last 2.5 min minus the average of the baseline registered preinhibitor treatment. Data are the means ± SEM of three independent experiments; ***$P \leq 0.0001$, **$P \leq 0.001$, and *$P \leq 0.05$ by one-way analysis of variance (ANOVA). (**C**) Normalized FRET ratios of PKC activity in COS7 cells coexpressing the indicated mCherry-tagged PKCη or mCherry empty vector and CKAR2. After establishing a baseline for 3 min, PKCs were activated with 100 μM UTP, after plateau cells were treated with 1 μM Gö6983. Data are representative of 38 to 52 cells per condition, from four independent experiments. (**D**) Relative PKC activity, quantified as area under the curve (AUC) from 3 to 11 min as a measure of signaling output. Data are the means ± SEM of four independent experiments; ***$P \leq 0.0001$, **$P \leq 0.001$, and *$P \leq 0.05$ by one-way ANOVA.

Enhanced Golgi-associated activity of PKCη K65R

Targeting of CKAR to specific intracellular locations has previously established that conventional PKC isozymes signal primarily at the plasma membrane, whereas PKC activity at the Golgi is mainly driven by the novel PKC isozymes (*21*). Therefore, we reasoned that the reduced activity of the PKCη variants measured using cytosolic CKAR could reflect enhanced activity at the Golgi, which would be sensed with Golgi-targeted CKAR. To test this, we coexpressed Golgi-targeted CKAR and mCherry-PKCη WT or each of the five variants in COS7 cells. The addition of Gö6983 revealed no significant difference in the basal activity of the variants compared to PKCη WT (Fig. 4, A and B). In cells expressing only the reporter, Gö6983 caused a reduction in the FRET ratio, reflecting the activity of endogenous novel PKC isozymes in COS7 cells (Fig. 4A, gray). However, the addition of Gö6983 after UTP stimulation revealed significantly higher PKC activity of the K65R mutant compared with WT (Fig. 4, C and D). Note that in these experiments, activity was normalized to the baseline after PKC inhibition. In cells first treated with UTP, the inhibitor-induced reduction in FRET was greater than that without UTP treatment because of activation-induced translocation of PKCη to the Golgi. These data show that the PKCη mutation K65R, identified as the most relevant *PRKCH* missense mutation in the AD GWAS, has enhanced agonist-induced signaling at the Golgi.

The K65R mutation does not alter the intrinsic catalytic activity or substrate binding of PKCη

We next examined the biochemical properties of the PKCη K65R variant to ascertain whether increased catalytic activity could account for its increased signaling output at the Golgi. Glutathione *S*-transferase (GST)–tagged PKCη WT or K65R were purified to homogeneity from insect cells using a baculovirus expression system (Fig. 5A). Western blot analysis revealed that both the WT and K65R proteins were processed by the priming phosphorylations at the activation loop (Thr^{513}), the turn motif (Thr^{656}), and the hydrophobic motif (Ser^{675}) (*22*) (Fig. 5A). Kinase assays revealed that the K65R mutant displayed indistinguishable activation kinetics from PKCη WT when assayed as a function of its two lipid activators, DG (half-maximal activation of 0.7 ± 0.1 mol% DG versus 0.5 ± 0.1 mol % DG for WT compared with mutant) or phosphatidylserine (PS; half-maximal activation at 3.3 ± 0.1 mol% PS versus 3.7 ± 0.2 mol% PS for WT compared with mutant), or as a function of the peptide substrate [Michaelis constant (K_m) of 18 ± 3 μM peptide versus 16 ± 3 μM peptide for WT versus mutant] (Fig. 5B). These data reveal that the K65R variant has the same degree of autoinhibition (activity was the same in the absence of DG), affinity for ligand (half-maximal activation achieved at the same mol fraction DG), affinity for anionic membranes (half-maximal activation achieved at the same mole % PS), and K_m for substrate as PKCη WT. These data establish that the mutation K65R does not alter the

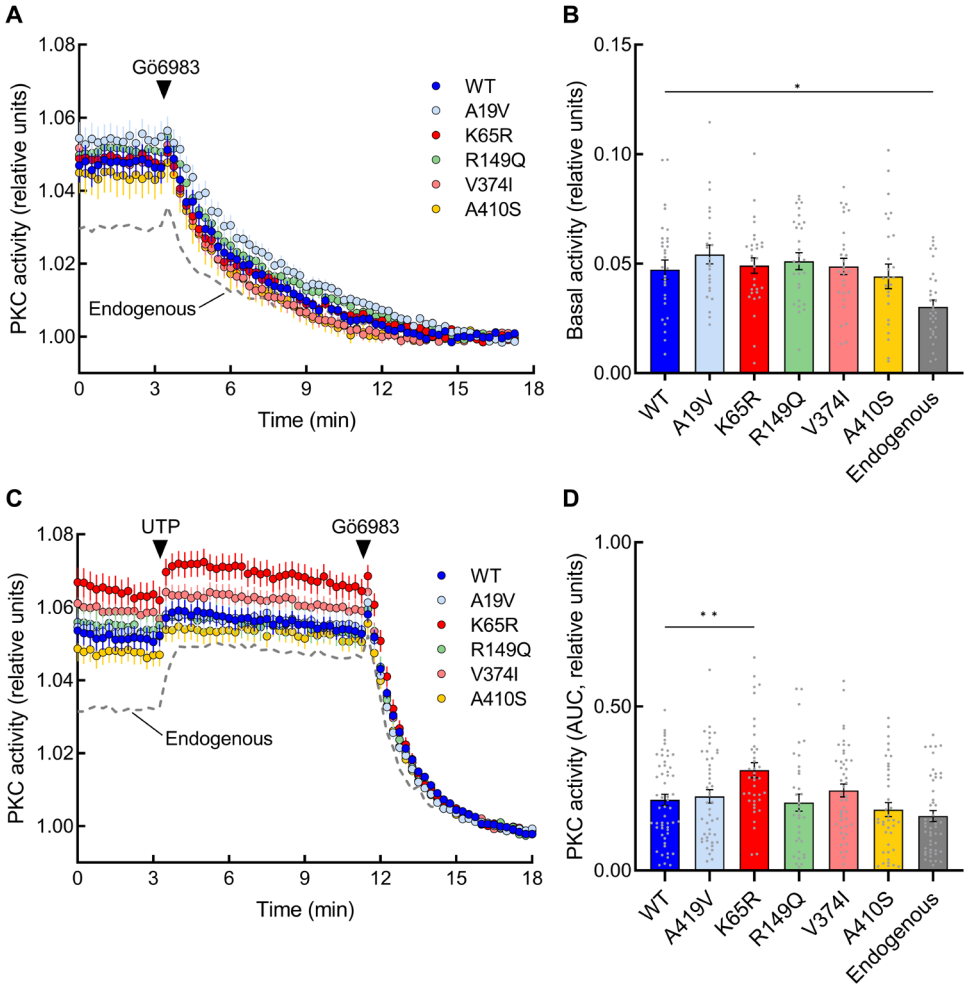

Fig. 4. PKCη K65R has enhanced activity at the Golgi. (**A**) Normalized FRET ratios representing PKC activity in COS7 cells coexpressing the indicated mCherry-tagged PKCη or mCherry empty vector (endogenous PKCs, grey trace) and the CKAR targeted to the Golgi. After 3 min, cells were treated with 1 μM Gö6983 to study PKC basal activity in the organelle. Data are representative of 26 to 30 cells per condition, from three independent experiments. (**B**) Relative basal activity quantified using the traces obtained in (A) by subtraction of the average of the last 2.5 min from the average of the baseline registered pretreatment. Data are the means ± SEM of three independent experiments; $*P \leq 0.05$ by one-way ANOVA. (**C**) Normalized FRET ratios of PKC activity in COS7 cells coexpressing the indicated mCherry-tagged PKCη or mCherry empty vector and the Golgi-CKAR. After 3 min, PKCs were activated with 100 μM UTP and subsequently inhibited with 1 μM Gö6983. Data are representative of 40 to 62 cells per condition, from four independent experiments. (**D**) Relative PKC activity, quantified as AUC from 3 to 11 min as a measure of signaling output. Data are the means ± SEM of four independent experiments; $**P \leq 0.001$ and $*P \leq 0.05$ by one-way ANOVA.

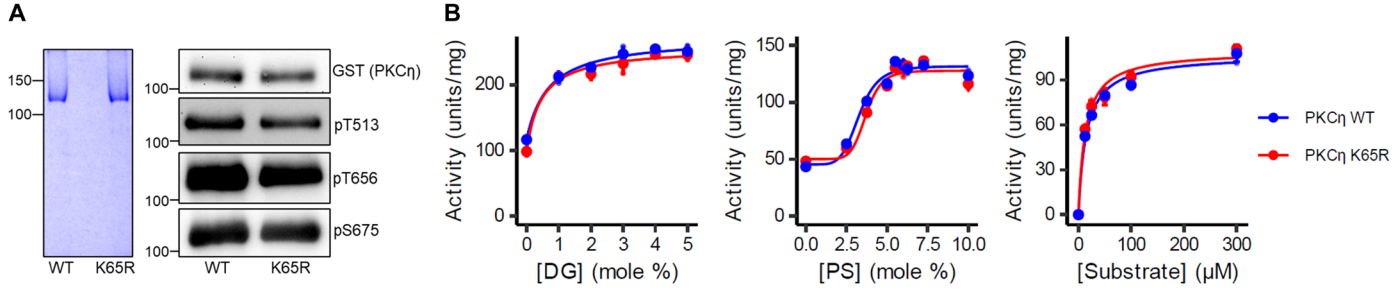

Fig. 5. K65R mutation does not alter the intrinsic catalytic properties of PKCη. (**A**) Left: Coomassie blue–stained SDS–polyacrylamide gel electrophoresis gel of purified GST-PKCη WT and GST-PKCη K65R. Right: Western blot of pure proteins probed with specific antibodies for total PKCη or the constitutive phosphorylation sites: the activation loop Thr^{513} (pT513), the turn motif Thr^{656} (pT656), and the hydrophobic motif Ser^{675} (pS675). (**B**) Activity of PKCη WT (blue) or K65R (red) (typically 2.4 nM) was measured as a function of mol% DG or PS or concentration of the peptide substrate, as described in Materials and Methods. Data are graphed in units (nmol phosphate per minute) per mg GST-PKC. Data represent the means ± SD of triplicate samples. Curves represent best nonlinear least squares fit as described in Materials and Methods.

intrinsic biochemical properties of PKCη. This is consistent with the residue being surface exposed and not involved in substrate binding or interdomain contacts that regulate the autoinhibition of the protein.

Enhanced Golgi localization of PKCη K65R compared with WT protein

Given that the AD variants are predicted to be on surface-exposed residues, we reasoned that altered interactions with binding partners could enhance localization of these enzymes to the Golgi. To assess this, we co-overexpressed mCherry-tagged PKCη WT or the AD mutants with the Golgi marker β-1,4-galactosyltransferase fused to monomeric enhanced green fluorescent protein (mEGFP) (Golgi-mEGFP) and examined their subcellular distribution by confocal microscopy (Fig. 6A). Colocalization analysis by Manders' coefficient (*23*), which measures the percentage of mCherry-labeled PKCη that colocalizes with the Golgi marker, revealed significantly increased Golgi

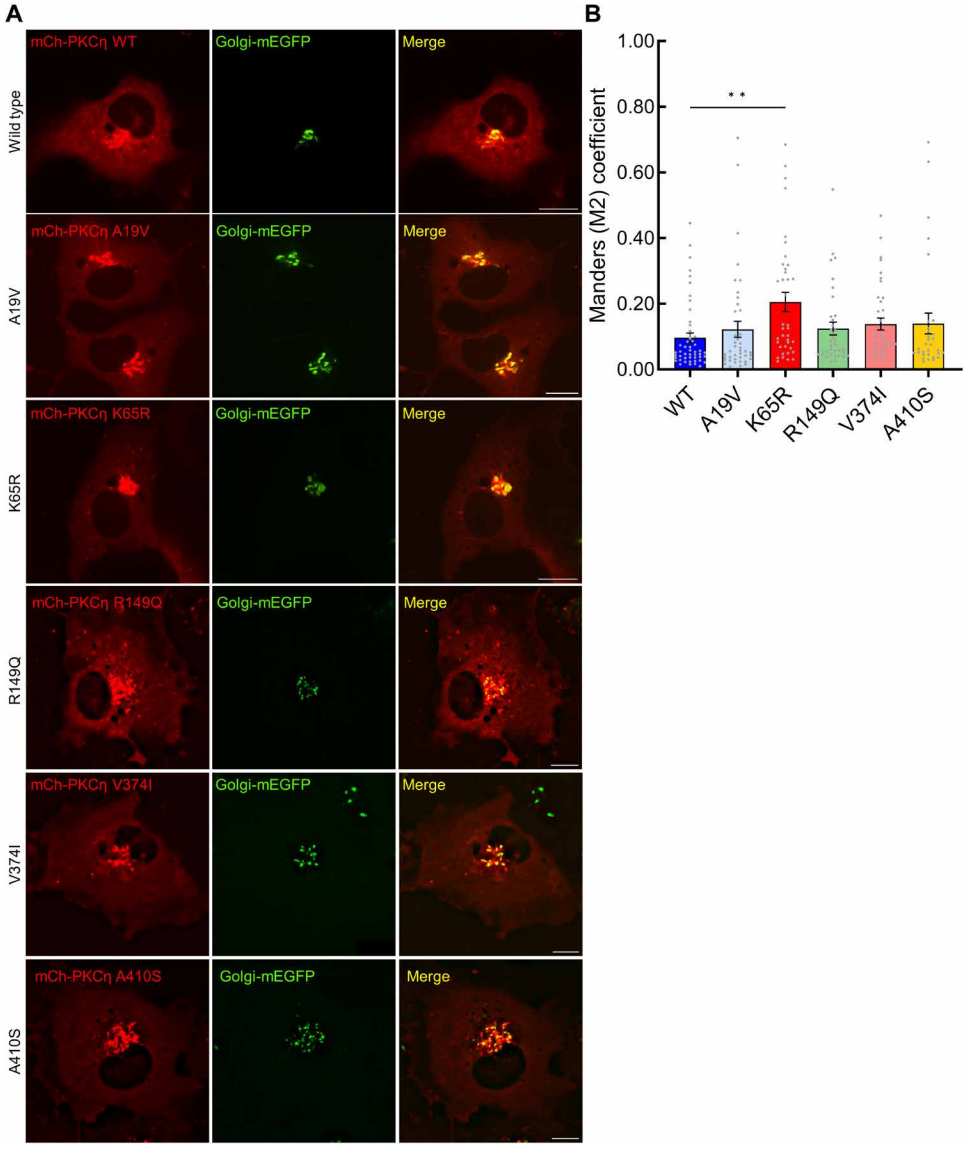

Fig. 6. Increased Golgi localization of PKCη K65R compared with WT protein. (**A**) Representative images from confocal microscopy of unstimulated COS7 cells expressing Golgi-mEGFP (green) together with mCherry-PKCη WT or the indicated AD variants (red). Scale bars, 10 μm. Images are representative of three independent experiments. (**B**) Bar graph indicating the M2 Mander's colocalization coefficients (*23*) for each mutant or WT PKCη and Golgi marker. Data are the means ± SEM of three independent experiments; $^{**}P = 0.002$ by one-way ANOVA.

localization of the K65R PKCη variant compared with PKCη WT (Fig. 6B). A trend toward increased Golgi localization was observed for each variant (Fig. 6B) but was only statistically significant for K65R. The increased localization of this AD variant with Golgi provides an explanation for its enhanced signaling at this organelle after agonist stimulation. It is noteworthy that the Golgi-localized CKAR did not reveal differences in basal activity of the AD variants. Whether the enhanced activity of variant PKCη at the Golgi is increasing the signaling output of cells remains to be determined.

We next assessed whether the increased agonist-evoked activity of PKCη K65R reflected increased agonist-stimulated translocation to the Golgi. We measured the translocation kinetics of yellow fluorescent protein (YFP)–tagged PKCη WT or the AD variants toward Golgi-tethered cyan fluorescent protein (CFP-Golgi) by monitoring the increase in FRET after UTP treatment of cells. Agonist treatment resulted in the greatest translocation to the Golgi of the K65R variant, with intermediate levels of translocation of A19V, R149Q, and A410S and the lowest translocation of WT and V374I (Fig. 7). Together, our results are consistent with the AD variants having enhanced affinity for the Golgi under basal conditions and enhanced translocation after stimulation, an effect most significant and pronounced for the PKCη K65R variant.

K65R mutation alters the interactome of PKCη

Given the enhanced Golgi localization of the K65R variant of PKCη, we reasoned that the interactome of the PKCη-AD–associated variant would differ from the WT protein one. We performed a proximity-dependent biotin identification (miniTurbo-ID) screen to compare the interactome of WT versus K65R in human embryonic kidney (HEK) cells, either before or after UTP treatment (*24*). More than 350 protein interactors were identified for PKCη that had differences in abundance between K65R and WT protein. Gene Ontology (GO) analysis revealed that Golgi-related processes were in the top 10 most significant biological processes based on the proteins, for which binding to PKCη K65R differed from that of WT (Fig. 8A). Abundant Golgi-localized proteins were associated

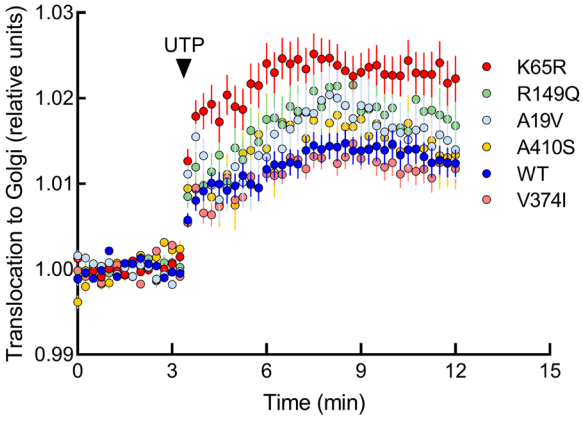

Fig. 7. PKCη K65R migrates more to the Golgi after UTP treatment. Traces indicate PKCη translocation to the Golgi in COS7 cells cotransfected with Golgi-CFP and the indicated YFP-PKCη. Translocation was monitored by measuring FRET/CFP ratio changes after stimulation with 100 μM UTP. Data for each cell were normalized to the average of the FRET before UTP addition and represent 27 to 55 cells per condition. Data are the means ± SEM of three independent experiments.

with the top 15 most significant biological processes (Fig. 8B), including signaling enzymes such as protein kinase D, structural proteins such as the Golgi matrix proteins GOLGA5 and GOLGA4, vesicle-trafficking proteins such as Sec22B and Sec24A, and Rab guanosine triphosphatases such as Rab29. These are primarily proteins associated with the cytoplasmic surface of the Golgi, where PKCη binds. GO analysis based on mammalian phenotypes (Fig. 8C) identified neurodegeneration as one of the top 10 most significant ontologies, with altered binding detected for proteins such as MARCKSL1 (Fig. 8D). The addition of UTP altered the interactome of both the WT and K65R PKCη, with differences between the effect on WT versus the AD variant. Notably, we identified groups of proteins that (i) only bound K65R upon UTP stimulation (Fig. 8E, dark gray), (ii) only bound WT upon UTP stimulation (Fig. 8E, medium gray), (iii) bound WT less but K65R more upon UTP stimulation (Fig. 8E, light gray), and (iv) bound WT more and K65R less upon UTP stimulation (Fig. 8E, white). These findings underscore the alteration in surface properties of the K65R mutation having a profound impact on the interactome of the AD variant compared with WT enzyme. Most notably, they indicate a large number of Golgi proteins and processes that are affected by the mutation.

Allele-specific *PRKCH* expression is increased in multiple brain regions

Last, the analysis of the Genotype-Tissue Expression (GTEx) database revealed increased expression of *PRKCH* in several brain tissue regions (most pronounced in the amygdala) for the recessive allele of rs7161410 (AA), which is in LD with the K65R mutation, compared with GA and GG alleles (1.087 versus −0.07720, −0.03857, respectively; fig. S2). Although not derived from AD samples per se, this up-regulation suggests a mechanism by which the variant may contribute to AD pathology. Assuming mRNA correlates with protein expression, this would support gain of function of K65R in AD, with our functional data indicating aberrantly high signaling at the Golgi.

DISCUSSION

We identified an intronic variant in the *PRKCH* gene strongly associated with AD risk and in strong LD with a rare missense mutation that alters PKCη function by strategically using a family-based GWAS of an RM using WGS from AD-affected families. Live-cell analysis revealed that several missense mutations in LD with the AD-associated *PRKCH* intronic variant risk allele exhibited reduced cellular basal activity in the cytosol; however, the genetically most relevant mutation, K65R, showed enhanced localization and signaling at the Golgi, as compared with WT PKCη (Fig. 9). The biochemical analysis of K65R revealed that the mutation did not alter its intrinsic biochemical properties. Rather, this mutation enhanced association of PKCη with Golgi and altered its interactome. These findings illustrate the power of family-based GWAS of WGS data using an RM to identify bona fide functional targets for AD.

By design, our GWAS could eliminate false-positive findings in terms of quality control and is robust to population stratification. In our analyses, the variants rs4420638 and rs56131196 were suggested as the most significant loci, which confirms the previously identified and well-known susceptibility region for AD on chromosome 19q13 (the *APOE* cluster gene region) (*25*, *26*). Along with *APOE*, our analysis showed that the association of *PRKCH* with AD-affected status was much stronger for a recessive versus additive inheritance model. Previously, we reported association of AD with rare-variant signals in *PRKCH* using single-variant and spatial-clustering analyses (*27*).

PKCη is primarily expressed in microglia as evidenced by the brain cell type–specific enhancer-promotor interactome map of active promoters (*28*). Microglia are a macrophage population in the brain and serve as the primary immune effector cells (*29*), and their dysregulation is associated with the pathogenesis of neurodegenerative diseases such as AD (*30*, *31*). In addition, dozens of AD-associated genes are known to affect microglial function in the brain (*32*). Notably, the phospholipase C γ gene, *PLCG2*, which produces DG to activate PKC, is a known AD risk gene that is highly expressed in microglia (*33*). Similarly, the AD risk factor TREM2 has been proposed to modulate the inflammatory signaling mediated by PKC (*33*, *34*).

The high expression of PKCη in microglia, coupled with its known role in immune and inflammatory signaling, poise this PKC isozyme in a prime position to regulate microglial-mediated inflammation, a key contributor to the progression of AD (*35*, *36*). Furthermore, a germline mutation, V374I, that increases the activity of PKCη is associated with stroke: The SNP rs2230500 is strongly associated with the risk of ischemic stroke or cerebral hemorrhage in the Asian population (*37*–*39*), which has a *P* of 0.011 (0.033 in NIMH only) with the same direction as rs7161410 in our AM analysis, despite the small affected family size. The correlation between stroke and AD (*40*) provides another link between deregulated PKCη function and AD. One plausible mechanism based on coronary arterial specimens suggested that PKCη is expressed in not only vascular endothelial cells but also white blood cells, of which foamy macrophages contribute to the cellular uptake of lipoproteins, mainly low-density lipoproteins (LDLs) (*37*, *41*). Amyloid-β also enhances cellular cholesterol accumulation by opsonization of LDL that accelerates macrophage foam cell formation (*41*). Therefore, PKCη signaling may be implicated in the potential participation of cerebral perivascular macrophages and microglia, leading to the disturbance of the cholesterol

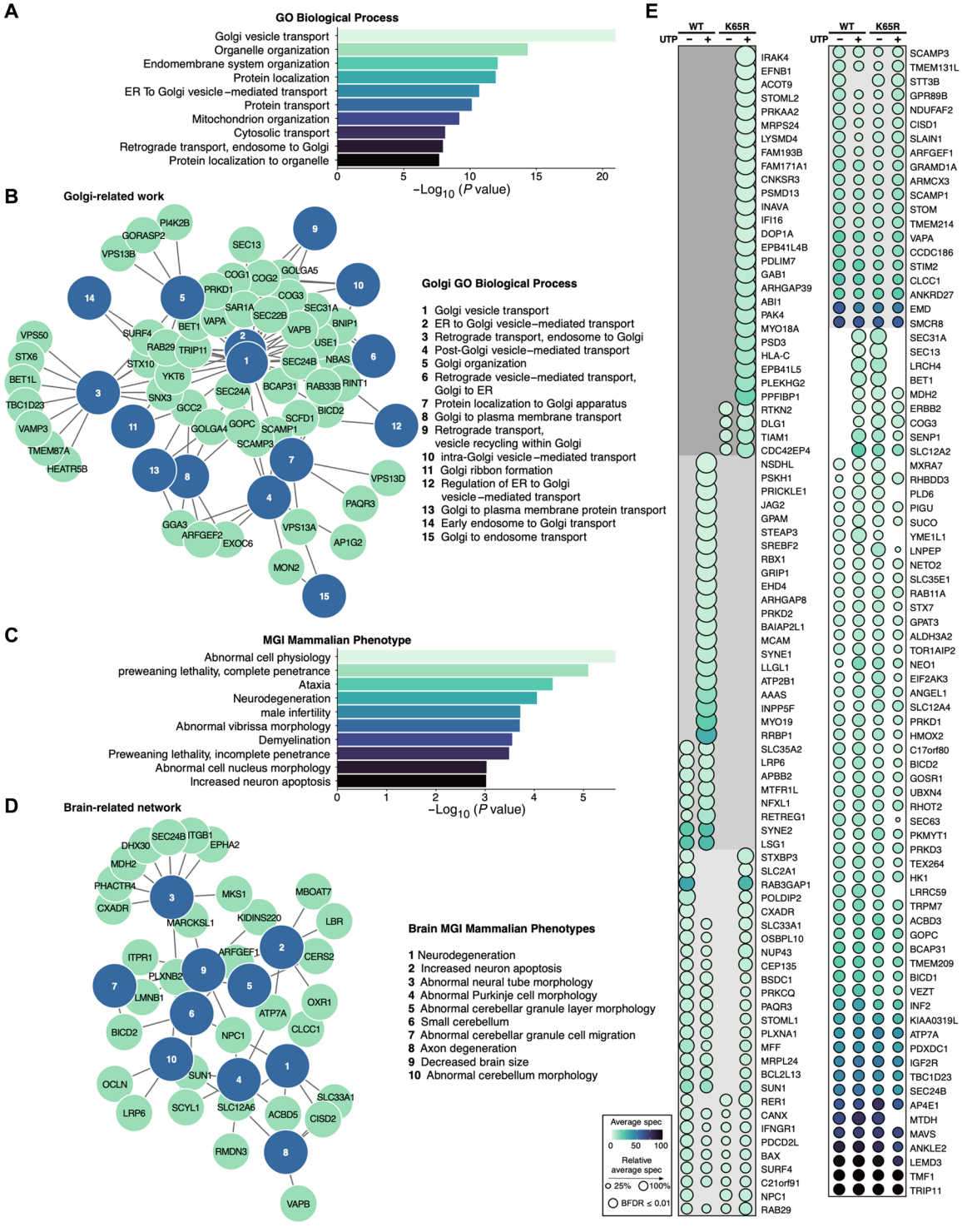

Fig. 8. Identification of PKCη WT and K65R protein interactors with miniTurboID. (**A** to **D**) GO enrichment analysis identified (A) the top 10 most significant ontologies and (B) 15 significant Golgi-related processes from GO Biological Process ($P \leq 0.05$) and (C) the top 10 most significant ontologies and (D) 10 significant brain-related phenotypes from MGI Mammalian Phenotypes ($P \leq 0.05$) for protein interactors altered between PKCη WT and K65R (BFDR ≤ 0.01). (**E**) Dot plot displays all protein interactors that have opposite changes in abundance with UTP compared with vehicle treatment between PKCη WT and K65R (different directionality is designated by grey shading). Colormap indicates abundance (average spectral count; spec), dot size indicates relative abundance, and outline color indicates BFDR ≤ 0.01.

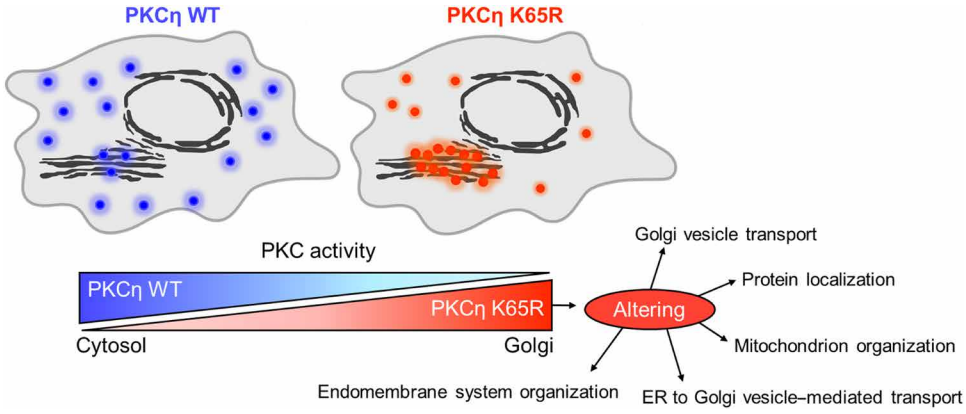

Fig. 9. Effects of K65R mutation compared with PKCη WT in subcellular localization, kinase activity, and cellular processes. A rare mutation in PKCη, K65R (linked to a recessively inherited intronic variant of *PRKCH* in family-based cohorts of AD), shifts the kinase's activity to the Golgi and increases its interactions with Golgi-associated proteins, thereby potentially altering Golgi-associated functions.

balance of brain tissues, thereby promoting amyloid accumulation and plaque generation. Last, a recent study revealed that PKCη is highly enriched in cortical astrocytes near amyloid plaques in the 5XFAD mouse model of AD, proposing that PKCη regulates neuroinflammation in AD (*42*). Thus, considerable evidence supports the possibility that restoring normal function of PKCη is a potential therapeutic target in AD.

This study is not without limitations. First, we acknowledge that the top recessive SNP, rs7161410, reached only suggestive genome-wide significance in our discovery dataset. We made several unsuccessful attempts to replicate this recessive signal in multiple other unrelated case-control cohorts and large biobanks. We note possible phenotype differences between family-based AD, sporadic AD in case-control cohorts, and AD-by-proxy or ICD10 in large biobanks and the limited availability of other family-based cohorts with multiplex AD families. Second, the rare functional mutation K65R (carriers of which were homozygous for rs7161410) was present in only one informative non-Hispanic white family, contributing to the rs7161410 signal. However, we observed nominal additive association for the functional mutation K65R in the latest NIA ADSP case-control dataset. In addition, we have shown experimentally how this functional mutation leads to enhanced localization and signaling of the protein at the Golgi. Given that the recessive rs7161410 signal was most pronounced in a subset of Dominican families, further functional research and replication attempts are necessary specifically in Dominican participants. Next, our biochemical and cellular studies in COS and HEK cells revealed that the K65R mutation in PKCη enhanced signaling at the Golgi and altered interaction with Golgi-associated proteins (Fig. 9). These data are consistent with a long history of reports on dysregulated Golgi structure and function in AD (*43, 44*). It is noteworthy that one of the proteins that displayed enhanced binding to K65R compared with WT was Rab29, which is associated with Parkinson's disease through its recruitment of the leucine rich repeat kinase 2 (LRRK2) (*45*). Future studies examining how PKCη regulates Golgi function, particularly in microglial cells, would be important to better understand how PKCη is a risk factor in AD. In addition, whether the intronic variant that first drew our attention to PKCη results in altered protein expression will be important to determine in order to understand how it confers a risk factor for AD.

In summary, the association of an intronic *PRKCH* variant with increased AD risk using an RM in a family-based GWAS of WGS data, along with a missense mutation in strong LD with the *PRKCH* variants' risk allele that alters PKCη signaling at the Golgi, suggests a previously unidentified biological link of AD etiology and neuropathogenesis with PKCη. Our results also support previous studies demonstrating a role for altered PKC signal activity in AD pathogenesis. Future studies aimed at understanding the mechanisms underlying abnormal localization and signaling of PKCη at the Golgi will be needed to help inform therapeutic strategies aimed at preventing and treating AD.

MATERIALS AND METHODS

Discovery WGS analysis

The samples from the NIMH AD Initiative were sequenced on the Illumina HiSeq 2000 platform and aligned to the human reference genome (GRCh38). Further details are discussed in (*46*). Sequencing data for the NIA cohort were obtained from the National Institute on Aging Genetics of Alzheimer's Disease Data Storage Site (NIAGADS) under accession no. NG00067.v9. A patient was considered to be affected if he/she was included in one of the following categories: definite AD, probable AD, or possible AD. Unaffected patients had either no dementia, suspected dementia (34 patients), or non-AD dementia (4 patients). Note that NIA ADSP families by design did not include individuals with two APOE-ε4 alleles. After standard quality control, both cohorts were merged. For variant quality control, we excluded multiallelic variants, monomorphic variants, singletons (variants with only one alternative allele across the dataset), indels, and variants, which had one missing allele among two alleles in an individual. The remaining variants were filtered on the basis of Mendel errors, genotyping rate (95%), and Hardy-Weinberg equilibrium ($P > 10^{-6}$). GWAS was conducted using the FBAT software (version 2.04) for RM and AM (*47*). We set the threshold for "suggestive" genome-wide statistical significance at $P < 5 \times 10^{-7}$. Although FBAT is robust to population structure and phenotype misspecification, we performed a stratified analysis by population. There were 412 patients of Dominican ancestry, 122 patients from a Dutch isolate group, 18 patients of Puerto Rican ancestry, 84 patients of African American ancestry, and the rest were of non-Hispanic white ancestry. For replication, we used unrelated case-control patients from three datasets: ADSP unrelated case-control patients (clinically defined AD phenotype), UK Biobank (AD-by-proxy phenotype), and All of Us (AD-by-proxy phenotype). Interaction analysis was performed using the "fbati" R package with the "fbatge" function.

Replication in the ADSP unrelated case-control dataset

We obtained WGS data for unrelated case controls from the NIAGADS webpage (ADSP R4). After sample quality control, the full dataset contained 25,660 patients (number of cases = 10,565). Subpopulations were defined using self-reporting and principal components (PCs), which were calculated on the basis of rare variants using the Jaccard index (*48*). Outliers more than five SDs away based on 10 PCs were excluded. In each subpopulation (European Americans, $N = 9609$, $N_{cases} = 6136$; African Americans, $N = 4263$, $N_{cases} = 1405$; Hispanic subpopulation, $N = 8466$, $N_{cases} = 2559$; Asian subpopulation, $N = 2543$, $N_{cases} = 181$), we performed a logistic regression using the RM or AM of inheritance for case/control status as implemented in PLINK 2 (*49*). We included sex, age, sequencing center, and five Jaccard PCs with standardized variance as covariates.

Replication in UK Biobank and the All of Us biobank

We used WGS data from 200,000 patients available in UK Biobank (*50*) and from 245,388 patients in All of Us (*51*). AD-by-proxy phenotype was defined as having family history of AD (at least one affected parent). Patients with unavailable information on family history were excluded. We performed a WGS regression with covariates as implemented in regenie (*52*). Step 1 was performed on SNPs from array data, and we followed the regenie recommendations (https://rgcgithub.github.io/regenie/recommendations). In step 2, we included age at enrollment, sex, 20 PCs, and sequencing center (available only in UK Biobank). PLINK 2 was used to extract the SNPs of interest. PCs for UK Biobank were provided. PCs for All of Us were obtained from an LD-pruned subset of SNPs using array data.

All participants provided electronically signed consent. UK Biobank received ethical approval from the NHS North West Centre for Research Ethics Committee with the latest renewal in 2021 (Ref: 11/NW/0382). Massachusetts General Hospital has a Data Use and Registration Agreement with All of Us. This study was approved by the relevant institutional review board from Massachusetts General Hospital (protocol numbers 2022P000614, 2015P000111, and 2019P001915).

Plasmids and reagents

The CKAR2 (*20*), Golgi-CKAR, and Golgi-CFP (*21*) plasmids were described previously. Human PKCη was YFP-, hemagglutinin-, or mCherry-tagged at the N terminus in pcDNA3 vectors using Gateway Cloning (Life Technologies). All AD-associated mutants were generated using QuickChange site-directed mutagenesis (Agilent), following the manufacturer's instructions. Golgi-mEGFP was obtained from AddGene (ID no. 182877). UTP trisodium salt was obtained from MerckMillipore (catalog no. 6701). Gö6983 (catalog no. 285) was purchased from Tocris. The anti-phosphorylated PKCη ($pThr^{655}$) antibody was purchased from Abcam (Ab5798), and pan antiphosphorylated PKC hydrophobic motif (βII pS660) antibody was from Cell Signaling Technology (9371S). The pan antiphosphorylated PKC activation loop antibody was previously described (*53*). The total PKCη (C-15, sc-215) and GST (B-14, sc-138) antibodies were purchased from Santa Cruz Biotechnology. Horseradish peroxidase–conjugated anti-rabbit (catalog no. 401315) and anti-mouse (catalog no. 401215) secondary antibodies and bovine serum albumin (BSA) (catalog no. 12659) were from Millipore. All antibodies were diluted in 1% BSA dissolved in PBS-T (1.5 mM sodium phosphate monobasic, 8 mM sodium phosphate dibasic, 150 mM NaCl, and 0.05% Tween 20) with 0.25 mM thimerosal (Thermo Fisher Scientific, catalog no. J61799.14). Bradford reagent (catalog no. 500-0006), protein standards ladder (catalog no. 161-0394), bis/acrylamide solution (catalog no. 161-0156), and polyvinylidene difluoride (catalog no. 162-0177) were purchased from Bio-Rad. Luminol (catalog no. A-8511) and *p*-coumaric acid (catalog no. C-9008) used to make the chemiluminescent substrate solution were purchased from Sigma-Aldrich. Lipids used in kinase assays (DG, 800811C and PS, 840034C) were from Avanti Polar Lipids.

Cell culture and transfection

COS7 cells were maintained in Dulbecco's modified Eagle's medium (Corning, catalog no. 10-013-CV) containing 10% fetal bovine serum (Atlanta Biologicals, catalog no. S11150) and 1% penicillin/streptomycin (Gibco, catalog no. 15-140-122) at 37°C in 5% CO_2. Cells were periodically tested for *Mycoplasma* contamination by a polymerase chain reaction–based method. Transient transfections were carried out using a Lipofectamine 3000 kit (Thermo Fisher Scientific) per the manufacturer's instructions, and constructs were allowed to express for 24 hours before imaging experiments.

FRET imaging and analysis

COS7 cells were seeded into plates (Corning, catalog no. 430165) containing glass cover slips (Fisherbrand, catalog no. 12545102) glued on using SYLGARD 184 Silicone Elastomer Kit (Dow, catalog no. 04019862). For CKAR assays, cells were cotransfected with 1 μg of mCherry-PKCη WT or each one of the PKCη AD-mutant constructs, together with 1 μg of CKAR2 or Golgi-CKAR DNA. For translocation assays, cells were cotransfected with 500 ng of YFP-tagged PKCη and 500 ng of Golgi-CFP. Twenty-four hours post-transfection, cells were imaged in 2 ml of Hank's balanced salt solution (Corning, catalog no. 21-022-CV) with 1 mM $CaCl_2$ added fresh before imaging. Images were acquired on a Zeiss Axiovert 200 M microscope (Carl Zeiss Micro-Imaging Inc.) using an Andor iXonUltra 888 digital camera (Oxford Instruments) controlled by MetaFluor software (Molecular Devices) version 7.10.1.161. Images were acquired every 15 s, and baseline images were acquired for 3 min. Drugs were added dropwise to the dish in between acquisitions. For CKAR (cytosolic and Golgi) activity assays, cells with equal mCherry and YFP levels were selected for analysis, and the FRET ratios for each cell were normalized to the average of the last 10 cycles. Basal activity was calculated as the subtraction of the average of the last 10 cycles from the first 3 min before the addition of the drug. For translocation assays, FRET ratios for each cell were normalized to the average of the first 3 min before drug treatment.

Confocal microscopy of live cells

COS7 cells were seeded onto MatTek glass-bottom culture dishes (catalog no. P35G-1.0-14-C); the next day, cells were transfected with 1 μg of Golgi-monomeric enhanced green fluorescent protein (Golgi-mEGPF) together with mCherry-PKCη WT or the AD mutants. After 24 hours, the live cells were imaged by confocal microscopy. Spinning disk confocal microscope specifications were as follows: Yokogawa X1 confocal scanhead mounted to a Nikon Ti2 microscope with a Plan apo lambda 100× oil numerical aperture 1.45 objective and microscope controlled via NIS Elements using the 405-, 488-, and 640-nm lines of a four-line (405, 488, 561, and 640 nm) LUN-F-XL laser engine and a Prime95B camera (Photometrics). Image channels were acquired using bandpass filters for each channel (455/50, 525/50, and 705/72). Images were analyzed

using NIS Elements software (Nikon), and JACoP plugin (*54*) in ImageJ (National Institutes of Health) was used to perform the colocalization analysis.

Quantification and statistical analysis

For imaging experiments, intensity values and FRET ratios were acquired using MetaFluor software and normalized as described above. Statistical tests were performed using Prism (GraphPad Software) version 9.5.0. Structures were modeled using PyMOL version 2.3.0 (Schrödinger, LLC).

Insect cell culture, protein purification, and kinase assays

Sf-9 insect cells were used to obtain baculoviruses expressing human GST-PKCη using the Bac-to-Bac expression system (Invitrogen). Human GST-PKCη WT and K65R proteins were expressed and purified with glutathione Sepharose beads as previously described (*55, 56*), with the following modifications. Cells were centrifuged, washed, and lysed in 50 mM Hepes (pH 7.5), 1 mM EDTA, 100 mM NaCl, 1% Triton X-100, 100 μM phenylmethylsulfonyl fluoride (PMSF), 1 mM dithiothreitol (DTT), 2 mM benzamidine, leupeptin (50 μg/ml), and 1 μM microcystin. The soluble lysate was incubated with glutathione resin beads (EMD Millipore, #70541-4) for 1 hour at 4°C on a nutator. Protein-bound beads were washed three times in wash buffer [50 mM Hepes (pH 7.5), 1 mM EDTA, 100 mM NaCl, and 1 mM DTT] and eluted five times in wash buffer with 10 mM glutathione. The purified protein was concentrated in 50-kDa Amicon centrifugal filter unit (EMD Millipore, #905024) and exchanged into 20 mM Hepes (pH 7.5), 1 mM EDTA, 1 mM EGTA, and 1 mM DTT. Glycerol was added to a final concentration of 50% for the proper storage of the enzyme at −20°C.

The activity of purified GST-PKCη (2.6 nM) was assayed toward a peptide substrate based on the predicted pseudosubstrate site of PKCη with a Ser in substitution of an Ala (Ac-RKRQRSMRRRVH-NH2, from GenScript). The kinase assay was performed as described previously (*55*), with the following changes in the protocol: the standard conditions of the assay were 100 μM adenosine 5′-triphosphate (ATP), [γ-32P] ATP (10 μCi/ml), 100 μM substrate, 5 mM $MgCl_2$, 500 μM EGTA, BSA (0.06 mg/ml), and Triton X-100 (0.1% w/v) mixed micelles containing 15 mol % PS and 5 mol % DG in 50 mM Hepes (pH 7.5) and 1 mM DTT. Mol% PS, mol% DG, and substrate concentration were adjusted as described in the figure legend. One unit of activity was defined as 1 nmol of phosphate incorporated per min into substrate. Kinase assay data were fit in R (version 4.4.2, 2024-10-31) using nonlinear least squares regression using the nls() command in the base package stats. Lipid activation curves were fit to a modified Hill equation of the form "$activity = a0 + (lipid^n) * (a1 - a0)/(lipid^n + k^n)$", where *a0* equals minimal (unstimulated) activity, *a1* equals maximal activity, lipid equals agonist concentration in mole percentage, *k* equals the agonist concentration at which half-maximal induced activity is realized, and *n* is the Hill coefficient (*57*). For DG curves, *n* was constrained to 1 to indicate the noncooperativity of this binding event. Substrate curves were fit to the Michaelis-Menten equation of the form "$activity = (Vmax * substrate)/(K_m + substrate)$", where *Vmax* indicates the maximal activity, *substrate* indicates the substrate concentration in micromolar, and K_m is the concentration of substrate at which the reaction rate is half of *Vmax*. Data were visualized using the R packages ggplot (version 3.5.1) and ggpubr (version 0.6.0).

eQTL analysis

We also explored the association between the variant and potential candidate genes by cis-expression quantitative trait loci in brain tissues based on the GTEx release version 8 database (www.gtexportal.org/home). This analysis was conducted specifically in postmortem brain tissues from individuals without diagnosed neurological disease (as per GTEx criteria). The R statistical software (www.R-project.org) was used to evaluate these tests.

MiniTurboID cell preparation and treatment

To generate the cell lines, pENTR-PKCη-WT or pENTR-PKCη-K65R constructs were fused to pDEST-pcDNA5-miniTurboID-3xFLAG-N-term via Gateway cloning (Thermo Fisher Scientific) following the manufacturer's specifications. These constructs were used to generate stable cell lines in HeLa Flp-In T-REx cell pools, as described in (*58*).

Stable cell lines (miniTurboID-PKCηWT, miniTurboID-PKCηK65R, miniTurboID empty vector, and parental cell line) were seeded in 15-cm dishes. When cells reached 80% confluency, cells were treated with doxycycline (1 mg/ml) for 24 hours to induce expression. All plates were then treated for 1 hour with 50 mM biotin, and half of them were treated with 100 mM UTP and the other half with ddH_2O as vehicle control. Cells were subsequently washed twice with ice-cold phosphate-buffered saline (PBS), collected with scrapper into 1.5 ml of PBS, and centrifuged at 500*g* for 5 min. Supernatants were carefully removed, and cell pellets were stored at −70°C until cell lysis.

Each frozen cell pellet was resuspended in ice-cold modified radioimmunoprecipitation assay (RIPA) lysis buffer [50 mM tris-HCl (pH 7.4) 150 mM NaCl, 1 mM EGTA, 0.5 mM EDTA, 1 mM $MgCl_2$, 1% NP-40, 0.1% SDS, 0.4% sodium deoxycholate, 1 mM PMSF, and 1x protease inhibitor cocktail] at a 1:4 pellet weight:volume ratio. Cells were sonicated for 15 s (5 s on, 3 s off for three cycles) at 30% amplitude on a sonicator with ⅛″ microtip. Samples were kept on ice. A total of 250 U of TurboNuclease and 10 μg of ribonuclease were added, and tubes were rotated (end-over-end) at 4°C for 15 min. Subsequently, SDS concentration was increased to 0.4% (by the addition of 10% SDS) and rotated at 4°C for 5 min. Lysates were centrifuged at 20,817*g* for 20 min at 4°C, and supernatant was transferred to a 2-ml centrifuge tube.

A master mix of streptavidin beads was prepared by using 35 μl of slurry (20-μl bed volume) for each sample plus 10% to account for any losses. Streptavidin Sepharose beads were washed three times with 1 ml of lysis buffer (minus proteinase inhibitors, PMSF, and deoxycholate). For bead washing, tubes were mixed by inversion and centrifuged at 400*g* for 1 min, and supernatant was discarded. After the last wash, beads were resuspended as a 50% slurry; 40 μl of the 50% slurry of streptavidin beads was added to the clarified supernatant and rotated using gentle end-over-end rotation for 3 hours at 4°C. Beads were pelleted by centrifugation at 400*g* for 1 min at 4°C, supernatant was discarded, and beads were transferred in 1 ml of fresh RIPA wash buffer [50 mM tris-HCl (pH 7.4), 150 mM NaCl, 1 mM EDTA, 1% NP-40, 0.1% SDS, and 0.4% sodium deoxycholate] to a new microcentrifuge tube (this removes "sticky" proteins bound to side of tube). Beads were washed once with SDS wash buffer [25 mM tris-HCl (pH 7.4) and 2% SDS], twice with RIPA wash buffer, once with TNNE buffer [25 mM tris-HCl (pH 7.4), 150 mM NaCl, 0.1% NP-40, and 1 mM EDTA], and three times with 50 mM ammonium bicarbonate (ABC) buffer (pH 8.0). For each wash step, tubes were

mixed by inversion and centrifuged at 400*g* for 1 min, and the supernatant was discarded.

Residual ABC buffer was removed by pipette, beads were resuspended in 70 μl of 50 mM ABC buffer, and 1 μg of trypsin dissolved in 50 mM ABC buffer was added and incubated at 37°C overnight with agitation. Additional 0.5 μg of trypsin was then added and incubated for a further 3 hours. Beads were centrifuged (400*g*, 2 min), and supernatants were collected in a new 1.5-ml tube. Beads were washed twice with 150 μl of mass spectrometry–grade H_2O (pelleting beads in between), and the wash supernatant was pooled with the peptide supernatant. Supernatants were centrifuged at 16,100*g* for 10 min, and most of the supernatant was transferred (leaving ~30 μl of residual so as not to transfer beads) to a new tube. The pooled supernatant was lyophilized using vacuum centrifugation without heat, and dried peptides were stored at −40°C until ready for mass spectrometry analysis.

MiniTurboID mass spectrometry analysis

Mass spectrometry analysis was performed in Bruker timsTOF Pro 2, using the method timsTOF dda-PASEF (22-min gradient-60SPD) for data-dependent acquisition (DDA) liquid chromatography tandem mass spectrometry; $^1/_{16}$ of digested peptides was analyzed using nano–high-performance liquid chromatography coupled to mass spectrometry. The sample ($^1/_{16}$) was loaded onto Evotip Pure per manufacturer's instructions. Peptides were eluted from the Performance column (catalog no. EV-1109, 8 cm by 150 μm with 1.5-μm beads, heated at 40°C) from a 20-μm-diameter emitter tip with the 60SPD preformed acetonitrile gradient generated by an Evosep One system and analyzed on a timsTOF Pro 2. MS1 scans were performed from 100 to 1700 Da in PASEF mode with an accumulation and ramp time of 100 ms (with four PASEF ramps and active exclusion at 0.4 min) and within the mobility range (1/K0) of 0.85 to 1.3 V·s/cm^2. The total cycle time was 0.53 s. The target intensity was set to 17,500, and intensity threshold was set to 1750; 1+ ions were excluded from fragmentation using a polygonal filter. The auto calibration was off.

To analyze the obtained data, files were searched with MSFragger (*59*) 3.7 within the ProHits (*60*) LIMS using FASTA database from UP000005640 human Uniprot (no isoforms). The data were searched for peptides digested with trypsin, with a maximum of two missed cleavages. Acetylated protein N-term and oxidated methionine were set as variable modifications with precursor and fragment mass tolerance set to 40 parts per million (ppm). MSBooster and Percolator were turned on. Percolator required a minimum probability of 0.5 and did not remove redundant peptides. The target-decoy competition method was used to assign *q* values and posterior error probabilities (PEPs). For ProteinProphet, the maximum peptide mass difference was set to 30 ppm. When generating the final report, the protein false discovery rate (FDR) filter was set to 0.01. FDR was estimated by using both filtered PSM and protein lists. Razor peptides were used for protein FDR scoring. All other parameters were default.

Significance Analysis of INTeractome (SAINT) software package was used to identify and score protein-protein interactions (*61*). SAINT was used to identify high-confidence protein interactors versus control samples. Before applying SAINT, proteins were filtered on the basis of unique peptides ≥ 2 to ensure confidence in identified proteins. Identified proteins had a Bayesian false discovery rate (BFDR) ≤ 0.01 and were considered high-confidence protein interactors. R programming was used for subsequent data processing (*62*). Protein interactors with altered abundance, measured as change in average spectral count, between genotypes (PKCη WT and PKCη K65R) and treatments (vehicle and UTP) were identified. GO enrichment analysis was performed for protein interactors that were altered between PKCη WT and PKCη K65R vehicle-treated groups using EnrichR to identify biological features from annotated gene databases, including GO Biological Process 2023 and MGI Mammalian Phenotypes Level 4 2021 (*63*–*67*). From the identified ontologies that showed significant enrichment for the protein interactors ($P \leq 0.05$), Golgi-related or brain-related ontologies were selected for visualization in a network analysis performed using Igraph (*68*). ProHits-viz was used to visualize protein-protein interaction data with dot plots. A representative dot plot displays protein interactors in which abundance was increased with UTP treatment in PKCη WT and decreased with UTP treatment in PKCη K65R and vice versa (*60*, *69*). Dots are absent in the plot for proteins that were below detection or failed to pass a BFDR ≤ 0.01.

Supplementary Materials

The PDF file includes:

Text S1
Figs. S1 and S2
Tables S1 to S3

Other Supplementary Material for this manuscript includes the following:

MDAR Reproducibility Checklist

REFERENCES AND NOTES

1. G. Livingston, J. Huntley, A. Sommerlad, D. Ames, C. Ballard, S. Banerjee, C. Brayne, A. Burns, J. Cohen-Mansfield, C. Cooper, S. G. Costafreda, A. Dias, N. Fox, L. N. Gitlin, R. Howard, H. C. Kales, M. Kivimäki, E. B. Larson, A. Ogunniyi, V. Orgeta, K. Ritchie, K. Rockwood, E. L. Sampson, Q. Samus, L. S. Schneider, G. Selbæk, L. Teri, N. Mukadam, Dementia prevention, intervention, and care: 2020 report of the Lancet Commission. *Lancet* **396**, 413–446 (2020).
2. T. S. Wingo, J. J. Lah, A. I. Levey, D. J. Cutler, Autosomal recessive causes likely in early-onset Alzheimer disease. *Arch. Neurol.* **69**, 59–64 (2012).
3. Y. Freudenberg-Hua, W. Li, P. Davies, The role of genetics in advancing precision medicine for Alzheimer's disease-a narrative review. *Front. Med.* **5**, 108 (2018).
4. I. E. Jansen, J. E. Savage, K. Watanabe, J. Bryois, D. M. Williams, S. Steinberg, J. Sealock, I. K. Karlsson, S. Hägg, L. Athanasiu, N. Voyle, P. Proitsi, A. Witoelar, S. Stringer, D. Aarsland, I. S. Almdahl, F. Andersen, S. Bergh, F. Bettella, S. Bjornsson, A. Brækhus, G. Bråthen, C. de Leeuw, R. S. Desikan, S. Djurovic, L. Dumitrescu, T. Fladby, T. J. Hohman, P. V. Jonsson, S. J. Kiddle, A. Rongve, I. Saltvedt, S. B. Sando, G. Selbæk, M. Shoai, N. G. Skene, J. Snaedal, E. Stordal, I. D. Ulstein, Y. Wang, L. R. White, J. Hardy, J. Hjerling-Leffler, P. F. Sullivan, W. M. van der Flier, R. Dobson, L. K. Davis, H. Stefansson, K. Stefansson, N. L. Pedersen, S. Ripke, O. A. Andreassen, D. Posthuma, Genome-wide meta-analysis identifies new loci and functional pathways influencing Alzheimer's disease risk. *Nat. Genet.* **51**, 404–413 (2019).
5. B. W. Kunkle, B. Grenier-Boley, R. Sims, J. C. Bis, V. Damotte, A. C. Naj, A. Boland, M. Vronskaya, S. J. van der Lee, A. Amlie-Wolf, C. Bellenguez, A. Frizatti, V. Chouraki, E. R. Martin, K. Sleegers, N. Badarinarayan, J. Jakobsdottir, K. L. Hamilton-Nelson, S. Moreno-Grau, R. Olaso, R. Raybould, Y. Chen, A. B. Kuzma, M. Hiltunen, T. Morgan, S. Ahmad, B. N. Vardarajan, J. Epelbaum, P. Hoffmann, M. Boada, G. W. Beecham, J.-G. Garnier, D. Harold, A. L. Fitzpatrick, O. Valladares, M.-L. Moutet, A. Gerrish, A. V. Smith, L. Qu, D. Bacq, N. Denning, X. Jian, Y. Zhao, M. D. Zompo, N. C. Fox, S.-H. Choi, I. Mateo, J. T. Hughes, H. H. Adams, J. Malamon, F. Sanchez-Garcia, Y. Patel, J. A. Brody, B. A. Dombroski, M. C. D. Naranjo, M. Daniilidou, G. Eiriksdottir, S. Mukherjee, D. Wallon, J. Uphill, T. Aspelund, L. B. Cantwell, F. Garzia, D. Galimberti, E. Hofer, M. Butkiewicz, B. Fin, E. Scarpini, C. Sarnowski, W. S. Bush, S. Meslage, J. Kornhuber, C. C. White, Y. Song, R. C. Barber, S. Engelborghs, S. Sordon, D. Voijnovic, P. M. Adams, R. Vandenberghe, M. Mayhaus, L. A. Cupples, M. S. Albert, P. P. De Deyn, W. Gu, J. J. Himali, D. Beekly, A. Squassina, A. M. Hartmann, A. Orellana, D. Blacker, E. Rodriguez-Rodriguez, S. Lovestone, M. E. Garcia, R. S. Doody, C. Munoz-Fernadez, R. Sussams, H. Lin, T. J. Fairchild, Y. A. Benito, C. Holmes, H. Karamujić-Čomić, M. P. Frosch, H. Thonberg,

W. Maier, G. Roshchupkin, B. Ghetti, V. Giedraitis, A. Kawalia, S. Li, R. M. Huebinger, L. Kilander, S. Moebus, I. Hernández, M. I. Kamboh, R. M. Brundin, J. Turton, Q. Yang, M. J. Katz, L. Concari, J. Lord, A. S. Beiser, C. D. Keene, S. Helisalmi, I. Kloszewska, W. A. Kukull, A. M. Koivisto, A. Lynch, L. Tarraga, E. B. Larson, A. Haapasalo, B. Lawlor, T. H. Mosley, R. B. Lipton, V. Solfrizzi, M. Gill, W. T. Longstreth Jr., T. J. Montine, V. Frisardi, M. Diez-Fairen, F. Rivadeneira, R. C. Petersen, V. Deramecourt, I. Alvarez, F. Salani, A. Ciaramella, E. Boerwinkle, E. M. Reiman, N. Fievet, J. I. Rotter, J. S. Reisch, O. Hanon, C. Cupidi, A. G. A. Uitterlinden, D. R. Royall, C. Dufouil, R. G. Maletta, I. de Rojas, M. Sano, A. Brice, R. Cecchetti, P. St. George-Hyslop, K. Ritchie, M. Tsolaki, D. W. Tsuang, B. Dubois, D. Craig, C.-K. Wu, H. Soininen, D. Avramidou, R. L. Albin, L. Fratiglioni, A. Germanou, L. G. Apostolova, L. Keller, M. Koutroumani, S. E. Arnold, F. Panza, O. Gkatzima, S. Asthana, D. Hannequin, P. Whitehead, C. S. Atwood, P. Caffarra, H. Hampel, I. Quintela, Á. Carracedo, L. Lannfelt, D. C. Rubinsztein, L. L. Barnes, F. Pasquier, L. Frölich, S. Barral, B. M. Guinness, T. G. Beach, J. A. Johnston, J. T. Becker, P. Passmore, E. H. Bigio, J. M. Schott, T. D. Bird, J. D. Warren, B. F. Boeve, M. K. Lupton, J. D. Bowen, P. Proitsi, A. Boxer, J. F. Powell, J. R. Burke, J. S. K. Kauwe, J. M. Burns, M. Mancuso, J. D. Buxbaum, U. Bonuccelli, N. J. Cairns, A. M. Quillin, C. Cao, G. Livingston, C. S. Carlson, N. J. Bass, C. M. Carlsson, J. Hardy, R. M. Carney, J. Bras, M. M. Carrasquillo, R. Guerreiro, M. Allen, H. C. Chui, E. Fisher, C. Masullo, E. A. Crocco, C. De Carli, G. Bisceglio, M. Dick, L. Ma, R. Duara, N. R. Graff-Radford, D. A. Evans, A. Hodges, K. M. Faber, M. Scherer, K. B. Fallon, M. Riemenschneider, D. W. Fardo, R. Heun, M. R. Farlow, H. Kölsch, S. Ferris, M. Leber, T. M. Foroud, I. Heuser, D. R. Galasko, I. Giegling, M. Gearing, M. Hüll, D. H. Geschwind, J. R. Gilbert, J. Morris, R. C. Green, K. Mayo, J. H. Growdon, T. Feulner, R. L. Hamilton, L. E. Harrell, D. Drichel, L. S. Honig, T. D. Cushion, M. J. Huentelman, P. Hollingworth, C. M. Hulette, B. T. Hyman, R. Marshall, G. P. Jarvik, A. Meggy, E. Abner, G. E. Menzies, L.-W. Jin, G. Leonenko, L. M. Real, G. R. Jun, C. T. Baldwin, D. Grozeva, A. Karydas, G. Russo, J. A. Kaye, R. Kim, F. Jessen, N. W. Kowall, B. Vellas, J. H. Kramer, E. Vardy, F. M. La Ferla, K.-H. Jöckel, J. J. Lah, M. Dichgans, J. B. Leverenz, D. Mann, A. I. Levey, S. Pickering-Brown, A. P. Lieberman, N. Klopp, K. L. Lunetta, H.-E. Wichmann, C. G. Lyketsos, K. Morgan, D. C. Marson, K. Brown, F. Martiniuk, C. Medway, D. C. Mash, M. M. Nöthen, E. Masliah, N. M. Hooper, W. C. M. Cormick, A. Daniele, S. M. M. Curry, A. Bayer, A. N. M. David, J. Gallacher, A. C. M. Kee, H. van den Bussche, M. Mesulam, C. Brayne, B. L. Miller, S. Riedel-Heller, C. A. Miller, J. W. Miller, A. Al-Chalabi, J. C. Morris, C. E. Shaw, A. J. Myers, J. Wiltfang, S. O'Bryant, J. M. Olichney, V. Alvarez, J. E. Parisi, A. B. Singleton, H. L. Paulson, J. Collinge, W. R. Perry, S. Mead, E. Peskind, D. H. Cribbs, M. Rossor, A. Pierce, N. S. Ryan, W. W. Poon, B. Nacmias, H. Potter, S. Sorbi, J. F. Quinn, E. Sacchinelli, A. Raj, G. Spalletta, M. Raskind, C. Caltagirone, P. Bossù, M. D. Orfei, B. Reisberg, R. Clarke, C. Reitz, A. D. Smith, J. M. Ringman, D. Warden, E. D. Roberson, G. Wilcock, E. Rogaeva, A. C. Bruni, H. J. Rosen, M. Gallo, R. N. Rosenberg, Y. Ben-Shlomo, M. A. Sager, P. Mecocci, A. J. Saykin, P. Pastor, M. L. Cuccaro, J. M. Vance, J. A. Schneider, L. S. Schneider, S. Slifer, W. W. Seeley, A. G. Smith, J. A. Sonnen, S. Spina, R. A. Stern, R. H. Swerdlow, M. Tang, R. E. Tanzi, J. Q. Trojanowski, J. C. Troncoso, V. M. Van Deerlin, L. J. Van Eldik, H. V. Vinters, J. P. Vonsattel, S. Weintraub, K. A. Welsh-Bohmer, K. C. Wilhelmsen, J. Williamson, T. S. Wingo, R. L. Woltjer, C. B. Wright, C.-E. Yu, L. Yu, Y. Saba, A. Pilotto, M. J. Bullido, O. Peters, P. K. Crane, D. Bennett, P. Bosco, E. Coto, V. Boccardi, P. L. De Jager, A. Lleo, N. Warner, O. L. Lopez, M. Ingelsson, P. Deloukas, C. Cruchaga, C. Graff, R. Gwilliam, M. Fornage, A. M. Goate, P. Sanchez-Juan, P. G. Kehoe, N. Amin, N. Ertekin-Taner, C. Berr, S. Debette, S. Love, L. J. Launer, S. G. Younkin, J.-F. Dartigues, C. Corcoran, M. A. Ikram, D. W. Dickson, G. Nicolas, D. Campion, J. A. Tschanz, H. Schmidt, H. Hakonarson, J. Clarimon, R. Munger, R. Schmidt, L. A. Farrer, C. Van Broeckhoven, M. C. O'Donovan, A. L. De Stefano, L. Jones, J. L. Haines, J.-F. Deleuze, M. J. Owen, V. Gudnason, R. Mayeux, V. Escott-Price, B. M. Psaty, A. Ramirez, L.-S. Wang, A. Ruiz, C. M. van Duijn, P. A. Holmans, S. Seshadri, J. Williams, P. Amouyel, G. D. Schellenberg, J.-C. Lambert, M. A. Pericak-Vance, Alzheimer Disease Genetics Consortium (ADGC), European Alzheimer's Disease Initiative (EADI), Cohorts for Heart and Aging Research in Genomic Epidemiology Consortium (CHARGE), Genetic and Environmental Risk in AD/Defining Genetic, Polygenic and Environmental Risk for Alzheimer's Disease Consortium (GERAD/PERADES), Genetic meta-analysis of diagnosed Alzheimer's disease identifies new risk loci and implicates Aβ, tau, immunity and lipid processing. *Nat. Genet.* **51**, 414–430 (2019).

6. Y. Takai, A. Kishimoto, U. Kikkawa, T. Mori, Y. Nishizuka, Unsaturated diacylglycerol as a possible messenger for the activation of calcium-activated, phospholipid-dependent protein kinase system. *Biochem. Biophys. Res. Commun.* **91**, 1218–1224 (1979).
7. Y. Nishizuka, Y. Takai, A. Kishimoto, E. Hashimoto, M. Inoue, M. Yamamoto, W. E. Criss, Y. Kuroda, A role of calcium in the activation of a new protein kinase system. *Adv. Cycl. Nucleotide Res.* **9**, 209–220 (1978).
8. A. C. Newton, Protein kinase C: Perfectly balanced. *Crit. Rev. Biochem. Mol. Biol.* **53**, 208–230 (2018).
9. G. Lordén, A. C. Newton, Conventional protein kinase C in the brain: Repurposing cancer drugs for neurodegenerative treatment? *Neuronal Signal* **5**, 1–10 (2021).
10. G. Sathe, K. K. Mangalaparthi, A. Jain, J. Darrow, J. Troncoso, M. Albert, A. Moghekar, A. Pandey, Multiplexed phosphoproteomic study of brain in patients with Alzheimer's disease and age-matched cognitively healthy controls. *OMICS* **24**, 216–227 (2020).
11. S. I. Alfonso, J. A. Callender, B. Hooli, C. E. Antal, K. Mullin, M. A. Sherman, S. E. Lesné, M. Leitges, A. C. Newton, R. E. Tanzi, R. Malinow, Gain-of-function mutations in protein kinase Cα (PKCα) may promote synaptic defects in Alzheimer's disease. *Sci. Signal.* **9**, ra47 (2016).
12. G. Lordén, J. M. Wozniak, K. Doré, L. E. Dozier, C. Cates-Gatto, G. N. Patrick, D. J. Gonzalez, A. J. Roberts, R. E. Tanzi, A. C. Newton, Enhanced activity of Alzheimer disease-associated variant of protein kinase Cα drives cognitive decline in a mouse model. *Nat. Commun.* **13**, 7200 (2022).
13. C. A. Pilo, T. R. Baffi, A. P. Kornev, M. T. Kunkel, M. Malfavon, D. H. Chen, L. A. Rossitto, D. X. Chen, L. C. Huang, C. Longman, N. Kannan, W. H. Raskind, D. J. Gonzalez, S. S. Taylor, G. Gorrie, A. C. Newton, Mutations in protein kinase Cγ promote spinocerebellar ataxia type 14 by impairing kinase autoinhibition. *Sci. Signal.* **15**, eabk1147 (2022).
14. J. P. Kapfhammer, E. Shimobayashi, Viewpoint: Spinocerebellar ataxias as diseases of Purkinje cell dysfunction rather than Purkinje cell loss. *Front. Mol. Neurosci.* **16**, 1182431 (2023).
15. D. Blacker, J. L. Haines, L. Rodes, H. Terwedow, R. C. P. Go, L. E. Harrell, R. T. Perry, S. S. Bassett, G. Chase, D. Meyers, M. S. Albert, R. Tanzi, ApoE-4 and age at onset of Alzheimer's disease: The NIMH genetics initiative. *Neurology* **48**, 139–147 (1997).
16. G. W. Beecham, J. C. Bis, E. R. Martin, S. H. Choi, A. L. DeStefano, C. M. van Duijn, M. Fornage, S. B. Gabriel, D. C. Koboldt, D. E. Larson, A. C. Naj, B. M. Psaty, W. Salerno, W. S. Bush, T. M. Foroud, E. Wijsman, L. A. Farrer, A. Goate, J. L. Haines, M. A. Pericak-Vance, E. Boerwinkle, R. Mayeux, S. Seshadri, G. Schellenberg, The Alzheimer's Disease Sequencing Project: Study design and sample selection. *Neurol. Genet.* **3**, e194 (2017).
17. T. J. Hoffmann, C. Lange, S. Vansteelandt, N. M. Laird, Gene-environment interaction tests for dichotomous traits in trios and sibships. *Genet. Epidemiol.* **33**, 691–699 (2009).
18. T. J. Hoffmann, S. Vansteelandt, C. Lange, E. K. Silverman, D. L. DeMeo, N. M. Laird, Combining disease models to test for gene-environment interaction in nuclear families. *Biometrics* **67**, 1260–1270 (2011).
19. A. C. Jones, S. S. Taylor, A. C. Newton, A. P. Kornev, Hypothesis: Unifying model of domain architecture for conventional and novel protein kinase C isozymes. *IUBMB Life* **72**, 2584–2590 (2020).
20. B. L. Ross, B. Tenner, M. L. Markwardt, A. Zviman, G. Shi, J. P. Kerr, N. E. Snell, J. J. McFarland, J. R. Mauban, C. W. Ward, M. A. Rizzo, J. Zhang, Single-color, ratiometric biosensors for detecting signaling activities in live cells. *eLife* **7**, e35458 (2018).
21. L. L. Gallegos, M. T. Kunkel, A. C. Newton, Targeting protein kinase C activity reporter to discrete intracellular regions reveals spatiotemporal differences in agonist-dependent signaling. *J. Biol. Chem.* **281**, 30947–30956 (2006).
22. L. M. Keranen, E. M. Dutil, A. C. Newton, Protein kinase C is regulated in vivo by three functionally distinct phosphorylations. *Curr. Biol.* **5**, 1394–1403 (1995).
23. E. M. M. Manders, F. J. Verbeek, J. A. Aten, Measurement of co-localization of objects in dual-colour confocal images. *J. Microsc.* **169**, 375–382 (1993).
24. T. C. Branon, J. A. Bosch, A. D. Sanchez, N. D. Udeshi, T. Svinkina, S. A. Carr, J. L. Feldman, N. Perrimon, A. Y. Ting, Efficient proximity labeling in living cells and organisms with TurboID. *Nat. Biotechnol.* **36**, 880–887 (2018).
25. V. K. Ramanan, S. L. Risacher, K. Nho, S. Kim, S. Swaminathan, L. Shen, T. M. Foroud, H. Hakonarson, M. J. Huentelman, P. S. Aisen, R. C. Petersen, R. C. Green, C. R. Jack, R. A. Koeppe, W. J. Jagust, M. W. Weiner, A. J. Saykin, for the Alzheimer's Disease Neuroimaging Initiative, APOE and BCHE as modulators of cerebral amyloid deposition: A florbetapir PET genome-wide association study. *Mol. Psychiatry* **19**, 351–357 (2014).
26. K. D. Coon, A. J. Myers, D. W. Craig, J. A. Webster, J. V. Pearson, D. H. Lince, V. L. Zismann, T. G. Beach, D. Leung, L. Bryden, R. F. Halperin, L. Marlowe, M. Kaleem, D. G. Walker, R. Ravid, C. B. Heward, J. Rogers, A. Papassotiropoulos, E. M. Reiman, J. Hardy, D. A. Stephan, A high-density whole-genome association study reveals that APOE is the major susceptibility gene for sporadic late-onset Alzheimer's disease. *J. Clin. Psychiatry* **68**, 613–618 (2007).
27. D. Prokopenko, S. L. Morgan, K. Mullin, O. Hofmann, B. Chapman, R. Kirchner, Alzheimer's Disease Neuroimaging Initiative (ADNI), S. Amberkar, I. Wohlers, C. Lange, W. Hide, L. Bertram, R. E. Tanzi, Whole-genome sequencing reveals new Alzheimer's disease-associated rare variants in loci related to synaptic function and neuronal development. *Alzheimers Dement.* **17**, 1509–1527 (2021).
28. A. Nott, I. R. Holtman, N. G. Coufal, J. C. M. Schlachetzki, M. Yu, R. Hu, C. Z. Han, M. Pena, J. Xiao, Y. Wu, Z. Keulen, M. P. Pasillas, C. O'Connor, C. K. Nickl, S. T. Schafer, Z. Shen, R. A. Rissman, J. B. Brewer, D. Gosselin, D. D. Gonda, M. L. Levy, M. G. Rosenfeld, G. McVicker, F. H. Gage, B. Ren, C. K. Glass, Brain cell type–specific enhancer–promoter interactome maps and disease-risk association. *Science* **366**, 1134–1139 (2019).
29. I. R. Holtman, D. Skola, C. K. Glass, Transcriptional control of microglia phenotypes in health and disease. *J. Clin. Invest.* **127**, 3220–3229 (2017).
30. V. H. Perry, J. A. R. Nicoll, C. Holmes, Microglia in neurodegenerative disease. *Nat. Rev. Neurol.* **6**, 193–201 (2010).
31. D. V. Hansen, J. E. Hanson, M. Sheng, Microglia in Alzheimer's disease. *J. Cell Biol.* **217**, 459–472 (2018).
32. M. Jorfi, A. Maaser-Hecker, R. E. Tanzi, The neuroimmune axis of Alzheimer's disease. *Genome Med.* **15**, 6 (2023).

33. R. Sims, S. J. van der Lee, A. C. Naj, C. Bellenguez, N. Badarinarayan, J. Jakobsdottir, B. W. Kunkle, A. Boland, R. Raybould, J. C. Bis, E. R. Martin, B. Grenier-Boley, S. Heilmann-Heimbach, V. Chouraki, A. B. Kuzma, K. Sleegers, M. Vronskaya, A. Ruiz, R. R. Graham, R. Olaso, P. Hoffmann, M. L. Grove, B. N. Vardarajan, M. Hiltunen, M. M. Nöthen, C. C. White, K. L. Hamilton-Nelson, J. Epelbaum, W. Maier, S.-H. Choi, G. W. Beecham, C. Dulary, S. Herms, A. V. Smith, C. C. Funk, C. Derbois, A. J. Forstner, S. Ahmad, H. Li, D. Bacq, D. Harold, C. L. Satizabal, O. Valladares, A. Squassina, R. Thomas, J. A. Brody, L. Qu, P. Sánchez-Juan, T. Morgan, F. J. Wolters, Y. Zhao, F. S. Garcia, N. Denning, M. Fornage, J. Malamon, M. C. D. Naranjo, E. Majounie, T. H. Mosley, B. Dombroski, D. Wallon, M. K. Lupton, J. Dupuis, P. Whitehead, L. Fratiglioni, C. Medway, X. Jian, S. Mukherjee, L. Keller, K. Brown, H. Lin, L. B. Cantwell, F. Panza, B. M. Guinness, S. Moreno-Grau, J. D. Burgess, V. Solfrizzi, P. Proitsi, H. H. Adams, M. Allen, D. Seripa, P. Pastor, L. A. Cupples, N. D. Price, D. Hannequin, A. Frank-García, D. Levy, P. Chakrabarty, P. Caffarra, I. Giegling, A. S. Beiser, V. Giedraitis, H. Hampel, M. E. Garcia, X. Wang, L. Lannfelt, P. Mecocci, G. Eiriksdottir, P. K. Crane, F. Pasquier, V. Boccardi, I. Henández, R. C. Barber, M. Scherer, L. Tarraga, P. M. Adams, M. Leber, Y. Chen, M. S. Albert, S. Riedel-Heller, V. Emilsson, D. Beekly, A. Braae, R. Schmidt, D. Blacker, C. Masullo, H. Schmidt, R. S. Doody, G. Spalletta, W. T. Longstreth Jr., T. J. Fairchild, P. Bossù, O. L. Lopez, M. P. Frosch, E. Sacchinelli, B. Ghetti, Q. Yang, R. M. Huebinger, F. Jessen, S. Li, M. I. Kamboh, J. Morris, O. Sotolongo-Grau, M. J. Katz, C. Corcoran, M. Dunstan, A. Braddel, C. Thomas, A. Meggy, R. Marshall, A. Gerrish, J. Chapman, M. Aguilar, S. Taylor, M. Hill, M. D. Fairén, A. Hodges, B. Vellas, H. Soininen, I. Kloszewska, M. Daniilidou, J. Uphill, Y. Patel, J. T. Hughes, J. Lord, J. Turton, A. M. Hartmann, R. Cecchetti, C. Fenoglio, M. Serpente, M. Arcaro, C. Caltagirone, M. D. Orfei, A. Ciaramella, S. Pichler, M. Mayhaus, W. Gu, A. Lleó, J. Fortea, R. Blesa, I. S. Barber, K. Brookes, C. Cupidi, R. G. Maletta, D. Carrell, S. Sorbi, S. Moebus, M. Urbano, A. Pilotto, J. Kornhuber, P. Bosco, S. Todd, D. Craig, J. Johnston, M. Gill, B. Lawlor, A. Lynch, N. C. Fox, J. Hardy, ARUK Consortium, R. L. Albin, L. G. Apostolova, S. E. Arnold, S. Asthana, C. S. Atwood, C. T. Baldwin, L. L. Barnes, S. Barral, T. G. Beach, J. T. Becker, E. H. Bigio, T. D. Bird, B. F. Boeve, J. D. Bowen, A. Boxer, J. R. Burke, J. M. Burns, J. D. Buxbaum, N. J. Cairns, C. Cao, C. S. Carlson, C. M. Carlsson, R. M. Carney, M. M. Carrasquillo, S. L. Carroll, C. C. Diaz, H. C. Chui, D. G. Clark, D. H. Cribbs, E. A. Crocco, C. De Carli, M. Dick, R. Duara, D. A. Evans, K. M. Faber, K. B. Fallon, D. W. Fardo, M. R. Farlow, S. Ferris, T. M. Foroud, D. R. Galasko, M. Gearing, D. H. Geschwind, J. R. Gilbert, N. R. Graff-Radford, R. C. Green, J. H. Growdon, R. L. Hamilton, L. E. Harrell, L. S. Honig, M. J. Huentelman, C. M. Hulette, B. T. Hyman, G. P. Jarvik, E. Abner, L.-W. Jin, G. Jun, A. Karydas, J. A. Kaye, R. Kim, N. W. Kowall, J. H. Kramer, F. M. La Ferla, J. J. Lah, J. B. Leverenz, A. I. Levey, G. Li, A. P. Lieberman, K. L. Lunetta, C. G. Lyketsos, D. C. Marson, F. Martiniuk, D. C. Mash, E. Masliah, W. C. M. Cormick, S. M. M. Curry, A. N. M. David, A. C. M. Kee, M. Mesulam, B. L. Miller, C. A. Miller, J. W. Miller, J. C. Morris, J. R. Murrell, A. J. Myers, S. O'Bryant, J. M. Olichney, V. S. Pankratz, J. E. Parisi, H. L. Paulson, W. Perry, E. Peskind, A. Pierce, W. W. Poon, H. Potter, J. F. Quinn, A. Raj, M. Raskind, B. Reisberg, C. Reitz, J. M. Ringman, E. D. Roberson, E. Rogaeva, H. J. Rosen, R. N. Rosenberg, M. A. Sager, A. J. Saykin, J. A. Schneider, L. S. Schneider, W. W. Seeley, A. G. Smith, J. A. Sonnen, S. Spina, R. A. Stern, R. H. Swerdlow, R. E. Tanzi, T. A. Thornton-Wells, J. Q. Trojanowski, J. C. Troncoso, V. M. Van Deerlin, L. J. Van Eldik, H. V. Vinters, J. P. Vonsattel, S. Weintraub, K. A. Welsh-Bohmer, K. C. Wilhelmsen, J. Williamson, T. S. Wingo, R. L. Woltjer, C. B. Wright, C.-E. Yu, L. Yu, F. Garzia, F. Golamaully, G. Septier, S. Engelborghs, R. Vandenberghe, P. P. De Deyn, C. M. Fernadez, Y. A. Benito, H. Thonberg, C. Forsell, L. Lilius, A. Kinhult-Stählbom, L. Kilander, R. M. Brundin, L. Concari, S. Helisalmi, A. M. Koivisto, A. Haapasalo, V. Dermecourt, N. Fievet, O. Hanon, C. Dufouil, A. Brice, K. Ritchie, B. Dubois, J. J. Himali, C. D. Keene, J. A. Tschanz, A. L. Fitzpatrick, W. A. Kukull, M. Norton, T. Aspelund, E. B. Larson, R. Munger, J. I. Rotter, R. B. Lipton, M. J. Bullido, A. Hofman, T. J. Montine, E. Coto, E. Boerwinkle, R. C. Petersen, V. Alvarez, F. Rivadeneira, E. M. Reiman, M. Gallo, C. J. O'Donnell, J. S. Reisch, A. C. Bruni, D. R. Royall, M. Dichgans, M. Sano, D. Galimberti, P. St. George-Hyslop, E. Scarpini, D. W. Tsuang, M. Mancuso, U. Bonuccelli, A. R. Winslow, A. Daniele, C.-K. Wu, GERAD/PERADES, CHARGE, ADGC, EADI, O. Peters, B. Nacmias, M. Riemenschneider, R. Heun, C. Brayne, D. C. Rubinsztein, J. Bras, R. Guerreiro, A. Al-Chalabi, C. E. Shaw, J. Collinge, D. Mann, M. Tsolaki, J. Clarimón, R. Sussams, S. Lovestone, M. C. O'Donovan, M. J. Owen, T. W. Behrens, S. Mead, A. M. Goate, A. G. Uitterlinden, C. Holmes, C. Cruchaga, M. Ingelsson, D. A. Bennett, J. Powell, T. E. Golde, C. Graff, P. L. De Jager, K. Morgan, N. Ertekin-Taner, O. Combarros, B. M. Psaty, P. Passmore, S. G. Younkin, C. Berr, V. Gudnason, D. Rujescu, D. W. Dickson, J.-F. Dartigues, A. L. De Stefano, S. Ortega-Cubero, H. Hakonarson, D. Campion, M. Boada, J. K. Kauwe, L. A. Farrer, C. Van Broeckhoven, M. A. Ikram, L. Jones, J. L. Haines, C. Tzourio, L. J. Launer, V. Escott-Price, R. Mayeux, J.-F. Deleuze, N. Amin, P. A. Holmans, M. A. Pericak-Vance, P. Amouyel, C. M. van Duijn, A. Ramirez, L.-S. Wang, J.-C. Lambert, S. Seshadri, J. Williams, G. D. Schellenberg, Rare coding variants in *PLCG2*, *ABI3*, and *TREM2* implicate microglial-mediated innate immunity in Alzheimer's disease. *Nat. Genet.* **49**, 1373–1384 (2017).
34. H. Yao, K. Coppola, J. E. Schweig, F. Crawford, M. Mullan, D. Paris, Distinct signaling pathways regulate TREM2 phagocytic and NFκB antagonistic activities. *Front. Cell. Neurosci.* **13**, 457 (2019).
35. S. C. Gray, K. J. Kinghorn, N. S. Woodling, Shifting equilibriums in Alzheimer's disease: The complex roles of microglia in neuroinflammation, neuronal survival and neurogenesis. *Neural Regen. Res.* **15**, 1208–1219 (2020).
36. J. W. Kinney, S. M. Bemiller, A. S. Murtishaw, A. M. Leisgang, A. M. Salazar, B. T. Lamb, Inflammation as a central mechanism in Alzheimer's disease. *Alzheimers Dement.* **4**, 575–590 (2018).
37. M. Kubo, J. Hata, T. Ninomiya, K. Matsuda, K. Yonemoto, T. Nakano, T. Matsushita, K. Yamazaki, Y. Ohnishi, S. Saito, T. Kitazono, S. Ibayashi, K. Sueishi, M. Iida, Y. Nakamura, Y. Kiyohara, A nonsynonymous SNP in PRKCH (protein kinase C eta) increases the risk of cerebral infarction. *Nat. Genet.* **39**, 212–217 (2007).
38. L. Wu, Y. Shen, X. Liu, X. Ma, B. Xi, J. Mi, K. Lindpaintner, X. Tan, X. Wang, The 1425G/A SNP in PRKCH is associated with ischemic stroke and cerebral hemorrhage in a Chinese population. *Stroke* **40**, 2973–2976 (2009).
39. J. Li, M. Luo, X. Xu, W. Sheng, Association between 1425G/A SNP in PRKCH and ischemic stroke among Chinese and Japanese populations: A meta-analysis including 3686 cases and 4589 controls. *Neurosci. Lett.* **506**, 55–58 (2012).
40. B. P. Lucke-Wold, R. C. Turner, A. F. Logsdon, J. W. Simpkins, D. L. Alkon, K. E. Smith, Y. W. Chen, Z. Tan, J. D. Huber, C. L. Rosen, Common mechanisms of Alzheimer's disease and ischemic stroke: The role of protein kinase C in the progression of age-related neurodegeneration. *J. Alzheimers Dis.* **43**, 711–724 (2015).
41. B. Schulz, G. Liebisch, M. Grandl, T. Werner, S. Barlage, G. Schmitz, Beta-amyloid (Abeta40, Abeta42) binding to modified LDL accelerates macrophage foam cell formation. *Biochim. Biophys. Acta* **1771**, 1335–1344 (2007).
42. A. Muraleedharan, N. Rotem-Dai, I. Strominger, N. P. Anto, N. Isakov, A. Monsonego, E. Livneh, Protein kinase C eta is activated in reactive astrocytes of an Alzheimer's disease mouse model: Evidence for its immunoregulatory function in primary astrocytes. *Glia* **69**, 697–714 (2021).
43. A. Stieber, Z. Mourelatos, N. K. Gonatas, In Alzheimer's disease the Golgi apparatus of a population of neurons without neurofibrillary tangles is fragmented and atrophic. *Am. J. Pathol.* **148**, 415–426 (1996).
44. G. Joshi, M. E. Bekier II, Y. Wang, Golgi fragmentation in Alzheimer's disease. *Front. Neurosci.* **9**, 340 (2015).
45. E. Purlyte, H. S. Dhekne, A. R. Sarhan, R. Gomez, P. Lis, M. Wightman, T. N. Martinez, F. Tonelli, S. R. Pfeffer, D. R. Alessi, Rab29 activation of the Parkinson's disease-associated LRRK2 kinase. *EMBO J.* **37**, 1–18 (2018).
46. D. Prokopenko, J. Hecker, R. Kirchner, B. A. Chapman, O. Hoffman, K. Mullin, W. Hide, L. Bertram, N. Laird, D. L. DeMeo, C. Lange, R. E. Tanzi, Identification of novel Alzheimer's disease loci using sex-specific family-based association analysis of whole-genome sequence data. *Sci. Rep.* **10**, 5029 (2020).
47. N. M. Laird, S. Horvath, X. Xu, Implementing a unified approach to family-based tests of association. *Genet. Epidemiol.* **19**, S36–S42 (2000).
48. D. Prokopenko, J. Hecker, E. K. Silverman, M. Pagano, M. M. Nöthen, C. Dina, C. Lange, H. L. Fier, Utilizing the Jaccard index to reveal population stratification in sequencing data: A simulation study and an application to the 1000 Genomes project. *Bioinformatics* **32**, 1366–1372 (2016).
49. C. C. Chang, C. C. Chow, L. C. A. M. Tellier, S. Vattikuti, S. M. Purcell, J. J. Lee, Second-generation PLINK: Rising to the challenge of larger and richer datasets. *Gigascience* **4**, 7 (2015).
50. C. Bycroft, C. Freeman, D. Petkova, G. Band, L. T. Elliott, K. Sharp, A. Motyer, D. Vukcevic, O. Delaneau, J. O'Connell, A. Cortes, S. Welsh, A. Young, M. Effingham, G. McVean, S. Leslie, N. Allen, P. Donnelly, J. Marchini, The UK Biobank resource with deep phenotyping and genomic data. *Nature* **562**, 203–209 (2018).
51. All of Us Research Program Investigators, J. C. Denny, J. L. Rutter, D. B. Goldstein, A. Philippakis, J. W. Smoller, G. Jenkins, E. Dishman, The "All of Us" Research Program. *N. Engl. J. Med.* **381**, 668–676 (2019).
52. J. Mbatchou, L. Barnard, J. Backman, A. Marcketta, J. A. Kosmicki, A. Ziyatdinov, C. Benner, C. O'Dushlaine, M. Barber, B. Boutkov, L. Habegger, M. Ferreira, A. Baras, J. Reid, G. Abecasis, E. Maxwell, J. Marchini, Computationally efficient whole-genome regression for quantitative and binary traits. *Nat. Genet.* **53**, 1097–1103 (2021).
53. E. M. Dutil, A. Toker, A. C. Newton, Regulation of conventional protein kinase C isozymes by phosphoinositide-dependent kinase 1 (PDK-1). *Curr. Biol.* **8**, 1366–1375 (1998).
54. S. Bolte, F. P. Cordelières, A guided tour into subcellular colocalization analysis in light microscopy. *J. Microsc.* **224**, 213–232 (2006).
55. J. A. Callender, Y. Yang, G. Lordén, N. L. Stephenson, A. C. Jones, J. Brognard, A. C. Newton, Protein kinase Cα gain-of-function variant in Alzheimer's disease displays enhanced catalysis by a mechanism that evades down-regulation. *Proc. Natl. Acad. Sci. U.S.A.* **115**, E5497–E5505 (2018).
56. I. S. Tobias, M. Kaulich, P. K. Kim, N. Simon, E. Jacinto, S. F. Dowdy, C. C. King, A. C. Newton, Protein kinase Cζ exhibits constitutive phosphorylation and phosphatidylinositol-3,4,5-triphosphate-independent regulation. *Biochem. J.* **473**, 509–523 (2016).

57. A. C. Newton, D. E. J. Koshland, High cooperativity, specificity, and multiplicity in the protein kinase C-lipid interaction. *J. Biol. Chem.* **264**, 14909–14915 (1989).
58. *Proteomics*: *Methods and Protocols*, vol. 1550 of *Methods in Molecular Biology*, L. Comai, J. E. Katz, P. Mallick, Eds. (Humana New York, 2017).
59. A. T. Kong, F. V. Leprevost, D. M. Avtonomov, D. Mellacheruvu, A. I. Nesvizhskii, MSFragger: Ultrafast and comprehensive peptide identification in mass spectrometry-based proteomics. *Nat. Methods* **14**, 513–520 (2017).
60. G. Liu, J. D. R. Knight, J. P. Zhang, C. C. Tsou, J. Wang, J. P. Lambert, B. Larsen, M. Tyers, B. Raught, N. Bandeira, A. I. Nesvizhskii, H. Choi, A. C. Gingras, Data independent acquisition analysis in ProHits 4.0. *J. Proteomics* **149**, 64–68 (2016).
61. G. Teo, G. Liu, J. Zhang, A. I. Nesvizhskii, A. C. Gingras, H. Choi, SAINTexpress: Improvements and additional features in Significance Analysis of INTeractome software. *J. Proteomics* **100**, 37–43 (2014).
62. R Core Team, *R A Language and Environment for Statistical Computing. R Foundation for Statistical Computing* (R Foundation for Statistical Computing, 2022); www.scirp.org/reference/referencespapers?referenceid=3456808.
63. M. Ashburner, C. A. Ball, J. A. Blake, D. Botstein, H. Butler, J. M. Cherry, A. P. Davis, K. Dolinski, S. S. Dwight, J. T. Eppig, M. A. Harris, D. P. Hill, L. Issel-Tarver, A. Kasarskis, S. Lewis, J. C. Matese, J. E. Richardson, M. Ringwald, G. M. Rubin, G. Sherlock, Gene Ontology: Tool for the unification of biology. *Nat. Genet.* **251**, 25–29 (2000).
64. E. Y. Chen, C. M. Tan, Y. Kou, Q. Duan, Z. Wang, G. V. Meirelles, N. R. Clark, A. Ma'ayan, Enrichr: Interactive and collaborative HTML5 gene list enrichment analysis tool. *BMC Bioinformatics* **14**, 128 (2013).
65. Gene Ontology Consortium, S. A. Aleksander, J. Balhoff, S. Carbon, J. M. Cherry, H. J. Drabkin, D. Ebert, M. Feuermann, P. Gaudet, N. L. Harris, D. P. Hill, R. Lee, H. Mi, S. Moxon, C. J. Mungall, A. Muruganugan, T. Mushayahama, P. W. Sternberg, P. D. Thomas, K. Van Auken, J. Ramsey, D. A. Siegele, R. L. Chisholm, P. Fey, M. C. Aspromonte, M. V. Nugnes, F. Quaglia, S. Tosatto, M. Giglio, S. Nadendla, G. Antonazzo, H. Attrill, G. D. Santos, S. Marygold, V. Strelets, C. J. Tabone, J. Thurmond, P. Zhou, S. H. Ahmed, P. Asanitthong, D. L. Buitrago, M. N. Erdol, M. C. Gage, M. A. Kadhum, K. Y. C. Li, M. Long, A. Michalak, A. Pesala, A. Pritazahra, S. C. C. Saverimuttu, R. Su, K. E. Thurlow, R. C. Lovering, C. Logie, S. Oliferenko, J. Blake, K. Christie, L. Corbani, M. E. Dolan, H. J. Drabkin, D. P. Hill, L. Ni, D. Sitnikov, C. Smith, A. Cuzick, J. Seager, L. Cooper, J. Elser, P. Jaiswal, P. Gupta, P. Jaiswal, S. Naithani, M. Lera-Ramirez, K. Rutherford, V. Wood, J. L. De Pons, M. R. Dwinell, G. T. Hayman, M. L. Kaldunski, A. E. Kwitek, S. J. F. Laulederkind, M. A. Tutaj, M. Vedi, S.-J. Wang, P. D'Eustachio, L. Aimo, K. Axelsen, A. Bridge, N. Hyka-Nouspikel, A. Morgat, S. A. Aleksander, J. M. Cherry, S. R. Engel, K. Karra, S. R. Miyasato, R. S. Nash, M. S. Skrzypek, S. Weng, E. D. Wong, E. Bakker, T. Z. Berardini, L. Reiser, A. Auchincloss, K. Axelsen, G. Argoud-Puy, M.-C. Blatter, E. Boutet, L. Breuza, A. Bridge, C. Casals-Casas, E. Coudert, A. Estreicher, M. L. Famiglietti, M. Feuermann, A. Gos, N. Gruaz-Gumowski, C. Hulo, N. Hyka-Nouspikel, F. Jungo, P. L. Mercier, D. Lieberherr, P. Masson, A. Morgat, I. Pedruzzi, L. Pourcel, S. Poux, C. Rivoire, S. Sundaram, A. Bateman, E. Bowler-Barnett, H. Bye-A-Jee, P. Denny, A. Ignatchenko, R. Ishtiaq, A. Lock, Y. Lussi, M. Magrane, M. J. Martin, S. Orchard, P. Raposo, E. Speretta, N. Tyagi, K. Warner, R. Zaru, A. D. Diehl, R. Lee, J. Chan, S. Diamantakis, D. Raciti, M. Zarowiecki, M. Fisher, C. James-Zorn, V. Ponferrada, A. Zorn, S. Ramachandran, L. Ruzicka, M. Westerfield, The Gene Ontology knowledgebase in 2023. *Genetics* **224**, iyad031 (2023).
66. Z. Xie, A. Bailey, M. V. Kuleshov, D. J. B. Clarke, J. E. Evangelista, S. L. Jenkins, A. Lachmann, M. L. Wojciechowicz, E. Kropiwnicki, K. M. Jagodnik, M. Jeon, A. Ma'ayan, Gene set knowledge discovery with Enrichr. *Curr. Protoc.* **1**, e90 (2021).
67. J. A. Blake, R. Baldarelli, J. A. Kadin, J. E. Richardson, C. L. Smith, C. J. Bult, the Mouse Genome Database Group, Mouse Genome Database (MGD): Knowledgebase for mouse–human comparative biology. *Nucleic Acids Res.* **49**, D981–D987 (2021).
68. G. Csárdi, T. Nepusz, The igraph software package for complex network research. *Complex Syst.* **1695**, 1–9 (2006).
69. J. D. R. Knight, G. Liu, J. P. Zhang, A. Pasculescu, H. Choi, A. C. Gingras, A web-tool for visualizing quantitative protein-protein interaction data. *Proteomics* **15**, 1432–1436 (2015).

Acknowledgments: We wish to thank C. Wong and L. McGary at the Network Biology Collaborative Centre Proteomics Facility for the miniTurboID analysis. We thank P. Guo and the Nikon Imaging Center at UCSD for support through the microscopy experiments. The computations in this paper were run in part on the FASRC Cannon cluster supported by the FAS Division of Science Research Computing Group at Harvard University. Please refer to the Supplementary Materials for the full acknowledgements (text S1). **Funding:** This work was supported in part by Cure Alzheimer's Fund (to C.L., A.C.N., and R.E.T.) and the National Institutes of Health grant R35 GM122523 (to A.C.N.). **Author contributions:** Conceptualization by C.L., A.C.N., and R.E.T. Methodology by M.C.G., D.P., S.L., S.A.W., J.H., G.H., D.L.D., W.H., L.B., C.L., A.C.N., and R.E.T. Investigation by M.C.G., D.P., S.L., S.A.W., J.H., J.W., M.W., G.L., J.E.M., Y.Y., I.C., S.M., G.H., D.L.D., W.H., L.B., C.L., A.C.N., and R.E.T. Funding acquisition by C.L., A.C.N., and R.E.T. Project administration by K.M. Supervision was provided by C.L., A.C.N., and R.E.T. Writing—the original was drafted by M.C.G., D.P., S.L., S.A.W., C.L., A.C.N., and R.E.T. and was revised and approved by M.C.G., D.P., S.L., S.A.W., J.H., J.W., M.W., G.L., J.E.M., Y.Y., I.C., K.M., S.M., G.H., D.L.D., W.H., L.B., C.L., A.C.N., and R.E.T. **Competing interests:** The authors declare that they have no competing interests. Furthermore, the funding body had no role in the design of the study; in the collection, analysis, and interpretation of data; or in writing the manuscript. **Data and materials availability:** The NIA ADSP WGS dataset is available from the NIAGADS data sharing service under accession number NG00067. The NIA ADSP dataset contains data in part obtained from the Alzheimer's Disease Neuroimaging Initiative (ADNI) database (adni.loni.usc.edu). As such, the investigators within the ADNI contributed to the design and implementation of ADNI and/or provided data but did not participate in analysis or writing of this report. Data from the genome-wide family-based recessive analysis of NIMH and NIA ADSP are available in Zenodo: https://doi.org/10.5281/zenodo.15729914. Uk Biobank data access is available through application at https://ukbiobank.dnanexus.com/landing. This research was conducted using the UK Biobank application number 81874. Access to individual-level data from the All of Us research program was obtained through an MGB-signed data use agreement with All of Us (www.researchallofus.org/register/). The mass spectrometry data were deposited in the MassIVE repository and assigned the accession number MSV000094742 (ftp://massive-ftp.ucsd.edu/v07/MSV000094742/). All other data needed to evaluate the conclusions in the paper are present in the paper or the Supplementary Materials.

Submitted 4 December 2024
Accepted 6 June 2025
Published 1 July 2025
10.1126/scisignal.adv0970